Atmos. Chem. Phys. Discuss., https://doi.org/10.5194/acp-2018-688
Manuscript under review for journal Atmos. Chem. Phys.
Discussion started: 6 August 2018

Atmospheric Chemistry and Physics Discussions

Structural changes in the shallow and transition branch of the Brewer-Dobson circulation induced by El Niño

Mohamadou Diallo[1,2], Paul Konopka[1], Michelle L. Santee[3], Rolf Müller[1], Mengchu Tao[1], Kaley A. Walker[4], Bernard Legras[2], Martin Riese[1], and Felix Ploeger[1]

[1]Institute of Energy and Climate Research, Stratosphere (IEK–7), Forschungszentrum Jülich, 52 425 Jülich, Germany.
[2]Laboratoire de Météorologie Dynamique, UMR8539, IPSL, UPMC/ENS/CNRS/Ecole Polytechnique, Paris, France.
[3]Jet Propulsion Laboratory, California Institute of Technology, Pasadena, California, USA.
[4]Department of Physics, University of Toronto, Toronto, Ontario, Canada.

Correspondence: Mohamadou Diallo (m.diallo@fz-juelich.de)

Abstract.

The stratospheric Brewer-Dobson circulation (BD-circulation) determines the transport and lifetime of key radiatively active trace gases and further impacts surface climate through downward coupling. Here, we quantify the variability in the lower stratospheric BD-circulation induced by the El Niño Southern Oscillation (ENSO), using satellite trace gas measurements and simulations with the Lagrangian chemistry transport model, CLaMS, driven by ERA-Interim and JRA-55 reanalyses. We show that despite discrepancies in the deseasonalised ozone (O_3) mixing ratios between CLaMS simulations and satellite observations, the patterns of changes in the lower stratospheric O_3 anomalies induced by ENSO agree remarkably well over the 2005–2016 period. Particularly during the most recent El Niño in 2015–2016, both satellite observations and CLaMS simulations show the largest negative tropical O_3 anomaly in the record. Regression analysis of different metrics of the BD-circulation strength, including mean age of air, vertical velocity, residual circulation and age spectrum, shows clear evidence for structural changes of the BD-circulation in the lower stratosphere induced by El Niño, consistent with observed O_3 anomalies. These structural changes during El Niño include a weakening of the transition branch of the BD-circulation between about 370–420 K (∼100–70 hPa) and equatorward of about 60° and, a strengthening of the shallow branch at the same latitudes and between about 420–500 K (∼70–30 hPa). The strengthening of the shallow branch induces negative tropical O_3 anomalies due to enhanced tropical upwelling, while the weakening of the transition branch combined with enhanced downwelling due to the strengthening shallow branch leads to positive O_3 anomalies in the extratropical upper troposphere-lower stratosphere (UTLS). Our results suggest that a shift of the ENSO basic state toward more frequent El Niño-like conditions in a warming future climate will substantially alter UTLS trace gas distributions due to these changes in the vertical structure of the stratospheric circulation.

Atmos. Chem. Phys. Discuss., https://doi.org/10.5194/acp-2018-688
Manuscript under review for journal Atmos. Chem. Phys.
Discussion started: 6 August 2018

Atmospheric Chemistry and Physics Discussions

1 Introduction

The lower stratosphere (10–25 km) is a key region in a changing climate. In this region, the amount of key greenhouse gases, such as water vapor and ozone, which radiatively impact temperatures both locally and globally, are regulated by advection, mixing, and chemistry (e.g. Forster and Shine, 2002, 1999; Solomon et al., 2010; Riese et al., 2012; Dessler et al., 2013). Ozone is a greenhouse gas ozone, which is mainly produced in the stratosphere (10–50 km), is directly regulated by the upwelling strength of the stratospheric circulation in the tropics.

The stratospheric mean meridional circulation, the so-called Brewer-Dobson circulation (BD-circulation) (e.g. Brewer, 1949; Butchart, 2014), is defined as a slow circulation in which air parcels rising in the tropics drift poleward in the stratosphere and, are transported downward at high latitudes via its shallow and deep branches (Bönisch et al., 2011; Lin and Fu, 2013). Driven by wave breaking in the stratosphere (Haynes et al., 1991; Rosenlof and Holton, 1993; Newman and Nash, 2000; Plumb, 2002) and varying on subseasonal to decadal timescales, the BD-circulation is modulated by natural variability (Plumb and Bell, 1982; Trepte and Hitchman, 1992; Niwano et al., 2003; Punge et al., 2009), including the El Niño Southern Oscillation (ENSO) (Randel et al., 2009).

ENSO is a coupled atmosphere-ocean phenomenon occurring in the equatorial Pacific Ocean with drastic changes in regional sea surface temperatures (SSTs), impacting surface weather and climate (e.g. Bjerknes, 1969; Cagnazzo and Manzini, 2009; Wang et al., 2016). ENSO alternates between anomalously warm (El Niño) and cold (La Niña) conditions in the tropical Eastern or Central Pacific Ocean at intervals of 2−8 years (Philander, 1990; Baldwin and O'Sullivan, 1995). El Niño and La Niña events are associated with variations in tropical SSTs, convection, and atmospheric temperature as well as in the circulation throughout the global troposphere (L'Heureux et al., 2017; Scaife et al., 2017). During El Niño, the Eastern equatorial or Central Pacific Ocean is anomalously warm and convection is shifted towards this region (e.g., Avery et al., 2017). During La Niña, in contrast, highest SSTs and most intense convection occur in the western Pacific. In either phase, the fluctuations associated with ENSO usually last for a little longer than one year. The oscillations in SSTs of the Pacific Ocean are accompanied by displacements of tropospheric temperature and precipitation patterns around the globe (Brönnimann et al., 2007).

ENSO is also a major mode of climate variability that affects the variability of the BD-circulation. Most of the previous research on ENSO influences on the stratosphere has concentrated on tropical and extratropical temperatures as well as on planetary waves in the extratropics and on polar vortex stability during El Niño based on global circulation models and observations (e.g., Sassi et al., 2004; Manzini et al., 2006; Taguchi and Hartmann, 2006; Garcia-Herrera et al., 2006; Garfinkel and Hartmann, 2007; Calvo et al., 2008; Ineson and Scaife, 2009; Butler et al., 2014). A substantial part of the interannual variability in the lower stratosphere turns out to be related to ENSO (Randel et al., 2009; Calvo et al., 2010). El Niño events directly warm the troposphere and cool the tropical lower stratosphere (including the tropopause region), suggesting a tropical coupling of the tropospheric and stratospheric variability (Calvo-Fernandez et al., 2004). Analyses of atmospheric temperatures from satellite observations indicated an overall warming of the tropical troposphere superimposed on equatorially symmetric subtropical Rossby wave gyres during El Niño events (Yulaeva and Wallace, 1994; Calvo-Fernandez et al., 2004). Using a comprehensive high-top general circulation model to investigate the dynamical mechanisms involved during ENSO winters, Simpson et al.

(2011) concluded that the response in tropical upwelling is predominantly driven by anomalous transient synoptic-scale wave drag in the southern hemisphere subtropical lower stratosphere. Based on zonally averaged satellite observations, Randel et al. (2009) found negative ozone and temperature anomalies in the tropical lower stratosphere attributed to strengthening tropical upwelling of the BD-circulation during El Niño events. In contrast, La Niña events induce an opposite zonal mean effect (e.g. Calvo et al., 2010; Konopka et al., 2016). Climate models shows that the ENSO modulations of the tropical upwelling appear to be linked to different propagation and dissipation patterns of parameterized gravity waves during winter (Garfinkel and Hartmann, 2008; Calvo et al., 2010; Simpson et al., 2011). According to Konopka et al. (2016), the variability of tropical upwelling in the lower stratosphere shows strong regional variations in the zonally resolved picture, especially during strong La Niña years when planetary wave activity at levels directly above the tropical tropopause is enhanced and the subtropical jets are significantly disturbed.

Most previous studies of direct ENSO influence on the BD-circulation have focused on changes in the strength of the tropical upwelling and on the mechanisms (wave-mean flow interaction) that produce its acceleration or deceleration (Randel et al., 2009; Calvo et al., 2010; Konopka et al., 2016). Here, we investigate the detailed changes in the vertical structure of different BD-circulation branches based on satellite observations and simulations with the Chemical Lagrangian Model of the Stratosphere (CLaMS) (McKenna et al., 2002; Konopka et al., 2004; Pommrich et al., 2014). Birner and Bönisch (2011) found a separation in the residual circulation transit times (RCTT) between the shallow and deep branches of the BD-circulation. In particular, they found much smaller transit times into the mid-latitude than into the polar lowermost stratosphere. Based on these findings, the shallow branch is found in the tropical stratosphere and in the lower mid-latitudinal stratosphere equatorward of about 60° below 30 hPa (∼500 K), whereas the deep branch is found throughout the high-latitude stratosphere poleward of 70° and above 30 hPa. In addition, Lin and Fu (2013) further separated the shallow branch defined by Birner and Bönisch (2011) into two sub-branches: the transition branch (i.e. lower part of the shallow branch between 100–70 hPa (370–420 K)) and the shallow branch (i.e. upper part of the previously defined shallow branch between 70–30 hPa (420–500 K)). Here, we use this definition of the branches to identify the "fingerprints" of the ENSO-induced variability in the structure of the BD-circulation. We disentangle the changes in each branch of the BD-circulation related to ENSO using multiple regression analysis on different diagnostic quantities derived from the satellite observations, CLaMS simulations and meteorology of two modern reanalysis products included in the SPARC Reanalysis Intercomparison Project (S-RIP) (Fujiwara et al., 2017). A description of the satellite observations, model data and the multiple regression technique is included in Section 2. Section 3 shows the ENSO impact on simulated and observed ozone mixing ratios in the lower stratosphere. Section 4 presents an analysis of the ENSO-induced changes in the vertical structure of the BD-circulation in the lower stratosphere, based on mean age of air, vertical velocity, residual circulation and age spectrum diagnostics. Finally, we discuss a possible dynamical mechanism for these changes in the vertical structure of the circulation and potential impacts on decadal and long-term changes (Sect. 5).

Atmos. Chem. Phys. Discuss., https://doi.org/10.5194/acp-2018-688
Manuscript under review for journal Atmos. Chem. Phys.
Discussion started: 6 August 2018

2 Data and Methodology

2.1 Description of the CLaMS model

The Chemical Lagrangian Model of the Stratosphere (CLaMS) is a Lagrangian transport model with trace gas transport based on the motion of 3-D forward trajectories and an additional parameterization of subgrid scale atmospheric mixing (McKenna et al., 2002; Konopka et al., 2004). CLaMS model allows ozone concentrations to be simulated through a simplified formulation of stratospheric chemistry (Pommrich et al., 2014). The lower boundary values for ozone mixing ratio are set to zero, while the boundary condition is imposed based on climatological satellite fields. For this study, we carried out simulations with CLaMS model driven by 6-hourly horizontal winds and diabatic heating rates both from ERA-Interim (ERA-I) (Dee et al., 2011) and Japanese 55-year Reanalysis (JRA-55) (Kobayashi et al., 2015) reanalyses, respectively provided by the European Centre for Medium-Range Weather Forecasts and the Japan Meteorological Agency. The simulations driven by ERA-I cover the 1979–2016, whereas the simulations driven by JRA-55 cover the 1979–2013 period. Both reanalyses are described in detail by Fujiwara et al. (2017) for the S-RIP project, which is a coordinated inter-comparison of modern global atmospheric reanalyses.

2.2 Lower stratospheric O_3 from CLaMS and Aura-MLS

To analyze the response of the BD-circulation to ENSO variability, we use ozone (O_3) mixing ratios and different diagnostics of the stratospheric circulation strength, as described in the following. The simulated O_3 mixing ratios from the CLaMS set-up used in this work were previously analysed by Pommrich et al. (2014) for validating the CLaMS simulations. Reliable agreement with satellite observations has been found regarding seasonality as well as variability related to the Quasi-Biennial Oscillation (QBO). The first part of the present analysis is a further validation of CLaMS' ability to reproduce interannual stratospheric variability related to ENSO.

The observational data used for comparison with CLaMS simulations are monthly mean O_3 mixing ratios in the lower stratosphere from the Aura Microwave Limb Sounder (MLS), covering the period 2005–2016 (Livesey et al., 2017). The MLS instrument, flying aboard the EOS-Aura satellite, is designed to measure a wide range of physical and chemical quantities, including O_3 (Waters et al., 2006). The version 4.2 of MLS data were produced with improved retrieval algorithms, which substantially reduced the occurrence of unrealistically small O_3 values at 215 hPa in the tropics observed in the previous version 2.2 MLS product (Livesey et al., 2008). Note that the version 4.2 of MLS data used here is not significantly different from the previous version 3.3 of MLS observations. The version 4.2 O_3 data are characterised by a vertical resolution of 2.5−3.5 km, a precision of ±0.02−0.1 ppmv, a systematic uncertainty ranging from ±0.01 ppmv±10% to 0.25 ppmv and a lowest recommended level of 261 hPa (Livesey et al., 2017; Santee et al., 2017). Additional detailed information on the quality of MLS O_3 in the upper troposphere-stratosphere in previous versions can be found in dedicated validation papers (Livesey et al., 2008; Froidevaux et al., 2008).

Atmos. Chem. Phys. Discuss., https://doi.org/10.5194/acp-2018-688
Manuscript under review for journal Atmos. Chem. Phys.
Discussion started: 6 August 2018

2.3 Metrics of the BD-circulation

In addition to the trace gas diagnostics, the strength of the BD-circulation is commonly deduced from age of air related diagnostics, including the mean age of air (AoA) and the age spectrum, and also with the residual vertical velocity ($\overline{w^*}$), the residual circulation transit time (RCTT) and the residual circulation mass stream function (ψ^*) (Reithmeier et al., 2008; Li et al., 2012; Diallo et al., 2012; Butchart, 2014; Abalos et al., 2015; Ploeger et al., 2015a, b; Ploeger and Birner, 2016). Mean AoA is defined as the averaged transit time for an air parcel since entering the stratosphere, and is therefore the first moment of the full transit time distribution termed the *age spectrum*. As shown by Hall and Plumb (1994), mean AoA can be calculated from a "clock-tracer" in a model that is an inert tracer with a linear increase in the troposphere or at the surface. Note that we calculate mean AoA and age spectrum relative to the lowest model level following the surface, as this is a common choice in global models (Waugh and Hall, 2002).

The age spectrum includes the detailed transit time information and is advantageous for investigating different transport pathways (e.g., Ploeger and Birner, 2016). In the CLaMS model, the age spectrum is calculated using a total of 60 different boundary pulse tracers, with pulses released in the lowest model layer in the tropics between 15° S and 15° N, constituting the pulse source region Ω at source times t'. For each pulse, the tracer mixing ratio $\chi_i(r,t)$ is set to unity in Ω for 30 days, and is set to zero in Ω otherwise. These pulses are released every two months, for instance, the first tracer pulse has its source time in January 1979, the second tracer pulse in March 1979, and so on. The age spectrum is a Green's function or a boundary propagator, G, that solves the continuity equation for the mixing ratio of a conserved and passive tracer (Hall and Plumb, 1994). As a function of transit time (elapsed time) $\tau = t - t'_i$, the age spectrum is constructed from these N pulse tracers at each sample field time t and sample region r as $G(r,t|\Omega, t-\tau_i) = \chi_i(r,t)$. For more details about the set-up and calculations see Ploeger and Birner (2016).

The residual circulation transit time (RCTT) is a 2-D diagnostic defined as the transit time of an air parcel through the stratosphere, if it was advected only by the residual circulation, and measures the strength of the residual circulation (Bönisch et al., 2011; Birner and Bönisch, 2011). RCTTs are calculated from 2-D CLaMS backward trajectories driven by the mass-weighted isentropic zonal mean diabatic circulation and the reference level is set to the 340 K isentrope in the tropics to include transport in the tropical tropopause layer (Fueglistaler et al., 2009a). For more details about the RCTT calculations see Ploeger et al. (2015a). In addition, we analyze the strength of the tropical upwelling related to ENSO using $\overline{w^*}$, calculated from the Transformed Eulerian Mean (TEM) circulation standard formula in geometric coordinates (e.g. equation (3.5), Andrews et al., 1987) and the diabatic heating rate (Fueglistaler et al., 2009b; Wright and Fueglistaler, 2013) from both reanalyses. In contrast to the integrated residual circulation transit time along the trajectory of an air parcel, $\overline{w^*}$ is a local 2-D quantity.

2.4 Multiple regression model

To properly disentangle the ENSO impact on these metrics of the BD-circulation from the other sources of natural variability, the monthly zonal mean O_3 mixing ratios and other diagnostic quantities, are analysed by using a multiple regression model as a function of latitude (ϕ) and altitude (z). This regression method is an established method and appropriate to disentangle

Atmos. Chem. Phys. Discuss., https://doi.org/10.5194/acp-2018-688
Manuscript under review for journal Atmos. Chem. Phys.
Discussion started: 6 August 2018

Atmospheric Chemistry and Physics Discussions

the relative influences of the considered climate indices on BD-circulation variability, as it includes time lag coefficients as a function of ϕ and z for each proxy, including ENSO. For more detail about the method and its further applications see Diallo et al. (2012, 2017, 2018). The regression method decomposes the temporal evolution of the monthly zonal mean parameter, χ, in terms of a long-term linear trend, seasonal cycle, QBO, ENSO, volcanic aerosol and a residual. The model yields for a given parameter, χ (herein O_3, AoA, $\overline{w^*}$, RCTT, Ψ, age spectrum, air mass fraction, temperature, zonal mean wind, Eliassen-Palm flux and its divergence)

$$\chi(t,\phi,z) = a(\phi,z)\cdot t + C(t,\phi,z) + \sum_{k=1}^{3} b_k(\phi,z)\cdot \mathrm{P}_k(t-\tau_k(\phi,z)) + \varepsilon(t,\phi,z) \quad (1)$$

where P_k represents the predictors or proxies of different atmospheric sources of variability. Thus, P_1 is a normalised QBO index (QBOi) from CDAS/Reanalysis zonally averaged winds at 50 hPa, P_2 is the normalised Multivariate ENSO Index (MEI) (Wolter and Timlin, 2011) and P_3 is the Aerosol Optical Depth (AOD) from satellite data (Vernier et al., 2011; Khaykin et al., 2017; Thomason et al., 2018). The coefficients are a linear trend a, the annual cycle $C(t,\phi,z)$, the amplitude b_1 and the lag $\tau_1(\phi,z)$ associated with the QBO, the amplitude b_2 and the lag $\tau_2(\phi,z)$ associated with ENSO and the amplitude b_3 and the lag $\tau_3(\phi,z)$ associated with AOD. The constraint applied to determine the parameters a, b_1, b_2, b_3, $\tau_1(\phi,z)$, $\tau_2(\phi,z)$, $\tau_3(\phi,z)$ and C is to minimise the residual $\varepsilon(t,\phi,z)$ in the least squares sense. Because of the presence of lags in the QBO, ENSO and AOD terms in equation (1), the problem is nonlinear and the residual may have multiple minima as a function of the parameters. In order to determine the optimal values of $\tau_1(\phi,z)$, $\tau_2(\phi,z)$ and $\tau_3(\phi,z)$, the residual is first minimised at fixed lag and then sorted out over a range of lags. This is done in sequence for QBO, ENSO and AOD. Here we neglect solar forcing, because our data set covers only one solar period. Uncertainty estimates for the statistical fits are calculated using a Student's t-test technique (Zwiers and von Storch, 1995; Bence, 1995; von Storch and Zwiers, 1999).

3 ENSO impact on lower stratospheric O_3

Figure 1(a, b) shows the interannual variability of the deseasonalised O_3 from CLaMS simulations (black line) and MLS observations (red line) averaged in the tropical lower stratosphere between 380–425 K as a percentage change relative to the climatological monthly mean mixing ratio during the 2005–2016 period. Generally, a consistent picture of O_3 internannual variability emerges between observations and model simulations for the 2005–2016 period. Note that the CLaMS O_3 values are twice larger than the MLS O_3 values in Fig. 1. The factor of 2 difference in the zonal mean magnitude between CLaMS and MLS O_3 anomalies is likely due to the lack of tropospheric O_3 chemistry and the O_3 lower boundary condition set to zero in CLaMS. The deseasonalised tropical O_3 time series exhibits seasonal variations in both model and observations, which are negatively correlated with the Multivariate ENSO Index (MEI) (Fig. 1a). In particular, during the 2015–2016 period, the deseasonalised O_3 shows negative anomalies in the tropical lower stratosphere due to the enhanced tropical upwelling caused by both the extreme El Niño event and the QBO disruption (e.g. easterly wind shear at 100–40 hPa) (Diallo et al., 2018).

Atmos. Chem. Phys. Discuss., https://doi.org/10.5194/acp-2018-688
Manuscript under review for journal Atmos. Chem. Phys.
Discussion started: 6 August 2018

Atmospheric Chemistry and Physics Discussions

However, the overall O_3 interannual variability is challenging to interpret because of its regulation by the complex interplay between the ENSO and QBO induced variability (Taguchi, 2010; Liess and Geller, 2012; Neu et al., 2014; Diallo et al., 2018). Therefore, to elucidate the ENSO impact on the stratospheric O_3 anomalies, the multiple regression is performed both without and with explicitly including the ENSO signal.The difference between the residual (ε in (1)) without and with explicit inclusion of the ENSO signal gives the ENSO-induced impact on stratospheric O_3 anomalies. This approach of differencing the residuals is similar to direct calculations, projecting the regression fits onto the ENSO basis functions herein termed as the *amplitude variation* ($b_2 \times STD(MEI)$ i.e. term b_2 in (1) normalised by the standard deviation of the MEI). For illustration, please see supplementary Fig. 2 and 4 in Diallo et al. (2017) and also in Diallo et al. (2018)).

Figure 1b shows time series of the O_3 changes induced by ENSO variability in the tropical lower stratosphere averaged between 380–425 K and estimated from the difference between the residual (ε in (1)) with and without explicit inclusion of the ENSO signal for the 2005–2016 period. This ENSO-induced variability in lower stratospheric O_3 mixing ratios between 380–425 K shows a strong negative correlation with the MEI, reaching -77.9% for CLaMS and -85.7% for MLS. Figures 2(a, b) show latitude-time series of the ENSO-induced variability in monthly mean O_3 mixing ratios in the lower stratosphere averaged between 380–425 K and estimated from the difference between the residual (ε in (1)) with and without explicit inclusion of the ENSO signal for the 2005–2016 period. The patterns of ENSO-induced variability in the two panels of Fig. 2 agree very well, though again with a factor of 2 difference in the magnitude related to the high biased O_3 variability in CLaMS consistent with Fig. 1b. The CLaMS and MLS O_3 anomalies are negative in the lower stratosphere during El Niño years (e.g., 2006–2007, 2010–2011, 2015–2016) and positive during La Niña years (e.g. 2008–2009, 2011–2012, 2013–2014), consistent with previous studies (Randel et al., 2009; Calvo et al., 2010; Konopka et al., 2016). In particular, the most recent El Niño event produces an extremely large negative O_3 anomaly in the lower stratosphere, inducing a record anomaly of minus 15 % in the tropics for MLS (twice as large for CLaMS), consistent with Diallo et al. (2018). This strong increase in negative O_3 anomalies is interpreted as a manifestation of the strengthening of the tropical upwelling induced by El Niño (see Sect. 4) (Randel et al., 2009). These substantial O_3 anomalies are consistent with recently published strong water vapor anomalies during the 2015–2016 El Niño (Avery et al., 2017; Diallo et al., 2018). The two consecutive La Niña events in 2011–2012 exhibit the largest positive O_3 anomalies in decadal satellite records.

Figures 3(a, b) depict the zonal mean impact of ENSO on O_3 variability for CLaMS (a) and MLS (b) calculated as the projection of the regression fits onto the ENSO basis functions for the 2005–2016 period, i.e. the amplitude variation. There is good agreement between CLaMS and MLS in the patterns of O_3 variations related to El Niño-like conditions. In the tropical UTLS, the negative O_3 anomalies during El Niño are due to the enhanced tropical upwelling, transporting upward fresh air poor in O_3 from the troposphere. In the extratropical UTLS (30°–70°), CLaMS model and MLS observations show a related positive O_3 anomaly due to enhanced downwelling (Neu et al., 2014). The negative O_3 anomalies seen in the southern hemisphere polar region are reflect large variability at high latitudes in Antarctic ozone (Solomon, 1999; WMO, 2014).

In addition, the O_3 anomalies induced by the ENSO signal indicate hemispheric asymmetry in both the simulations and the observations, with a generally weaker response in the southern hemisphere compared to the northern hemisphere in MLS. Note that the absence of O_3 anomalies above 500 K in CLaMS (Fig. 3a) results from the upper boundary condition, which

Atmos. Chem. Phys. Discuss., https://doi.org/10.5194/acp-2018-688
Manuscript under review for journal Atmos. Chem. Phys.
Discussion started: 6 August 2018

Atmospheric Chemistry and Physics Discussions

is imposed based on climatological fields and thus precludes representation of variability. Despite general agreement between model and observations, the signal in the MLS data is weaker in both the tropics and the extratropics, particularly in the southern hemisphere. The stratospheric entry value of fire emission markers is strongly enhanced under El Niño conditions (Fromm and Servranckx, 2003; Fromm et al., 2006; Trentmann et al., 2006). Increased upper tropospheric O_3 mixing ratios have also been linked to increased O_3 precursor emissions from biomass burning. The dynamical changes, severe drought, and ensuing large-scale forest fires in Indonesia and Malaysia induced by strong El Niño events have been conclusively associated with substantial anomalies in UTLS CO and O_3 (e.g. Thompson et al., 2001; Logan et al., 2008; Chandra et al., 2007, 2009; Nassar et al., 2009; Livesey et al., 2013; Field et al., 2016). Thus, tropical upper tropospheric O_3 mixing ratios may be enhanced not only because of increased convective transport but also increased fire emissions (this was especially true in 2015 Field et al., 2016). Hence, the tropical UTLS O_3 mixing ratios will reflect the net change from competing effects that CLaMS simulations cannot capture because of the use of zero O_3 as a lower boundary condition, as mentioned earlier. In some cases these local/regional effects may have been large enough to impact the tropical mean O_3 mixing ratios. In the CLaMS model this chemical relationship between CO and O_3 is missing, which might explaining the discrepancies with MLS observations.

4 Structural changes in the lower stratospheric BD-circulation

In this section, various diagnostics of the BD-circulation strength (e.g., AoA, $\overline{w^*}$, Ψ, RCTT, age spectrum) from simulations with CLaMS, driven by ERA-I and JRA-55 reanalyses, are analyzed for ENSO-related variability and consistency with the O_3-based results (see Sect. 3). In contrast to the complex chemistry in trace gases, the AoA is particularly useful as a diagnostic for investigating variability in stratospheric transport and mixing, as it is not influenced by chemistry.

Figures 4(a-b) show the amplitude variation of the ENSO impact on AoA for the 1979–2013 period. The vertical structure of AoA anomalies depicts a pattern of changes similar to the ENSO imprint on O_3 mixing ratios. Negative AoA anomalies (young AoA) emerge throughout the tropics in both ERA-I and JRA-55 reanalyses and propagate upwards into the stratosphere during El Niño-like conditions. Positive AoA anomalies (old AoA) arise in the extratropics with a strong effect in the northern hemisphere during El Niño. The picture of negative AoA anomalies in the tropical lower stratosphere and positive AoA anomalies in the mid and high latitudes (30°–60° N and S) agrees well with O_3 anomalies from CLaMS simulations and MLS observations (Fig. 3). Figures 4(c, d) depict the ENSO-induced variability in the $\overline{w^*}$, indicating a clear increase in the tropical upwelling during El Niño-like conditions and consistent with recent findings (Randel et al., 2009; Calvo et al., 2010; Konopka et al., 2016). The vertical structures of AoA and O_3 changes in the UTLS, i.e., negative anomalies in the tropics and positive anomalies in the extratropics during El Niño-like conditions, is mainly explained by the ENSO-induced anomalies in $\overline{w^*}$ and in the diabatic heating rate ($\dot{\Theta}$) (Fig. 4(c-f)). During El Niño, the increase of the ascending branch of the BD-circulation (positive tropical $\overline{w^*}$ and $\dot{\Theta}$) transports upward more young upper tropospheric air poor in O_3 into the tropical stratosphere, while the enhanced downwelling in the mid and high latitudes transports more old stratospheric air rich in O_3 downwards into the polar regions (see Fig. 3). Consequently, the enhanced tropical upwelling depletes O_3 in the tropical lower stratosphere, while the strengthened downwelling enhances O_3 in the mid and high latitudes. Opposite changes occur during La Niña (not shown).

Atmos. Chem. Phys. Discuss., https://doi.org/10.5194/acp-2018-688
Manuscript under review for journal Atmos. Chem. Phys.
Discussion started: 6 August 2018

Atmospheric Chemistry and Physics Discussions

The ENSO-induced variations in $\overline{w^*}$ and $\dot{\Theta}$ agree well in the two reanalyses in terms of morphology, though not in magnitude. The $\overline{w^*}$ and $\dot{\Theta}$ related to El Niño for JRA-55 are more confined in the tropics and exhibit stronger downwelling in the northern hemisphere than ERA-I.

However, as the AoA is affected by both residual circulation and mixing processes (Garny et al., 2014; **?**; Ploeger et al., 2015a), there could be an ambiguous relation between AoA changes and upwelling or downwelling. Therefore, we also analyse the ENSO-induced RCTT and ψ^* anomalies (Fig. 5(a–d)). The ENSO impact on the vertical structure of the BD-circulation becomes evident from the mass stream function and the RCTT, i.e. the time scale of transport by the pure residual circulation (Fig. 5). In the tropical lower stratosphere, El Niño causes decreasing RCTT throughout most parts of the stratosphere (below 550 K) related to the strengthening tropical residual circulation cell associated with the shallow branch of the BD-circulation (Birner and Bönisch, 2011). The strengthening tropical residual circulation in Fig. 5(a, b) is consistent with positive (negative) stream function changes in the northern hemisphere (southern hemisphere), indicating a strengthening residual mean mass circulation in the tropics (Fig. 5(c, d)). In the extratropical lower stratosphere at altitudes below 450 K, the RCTT increases during El Niño, consistent with a weakening extratropical residual circulation cell related to the transition branch of the BD-circulation (Lin and Fu, 2013). These changes in extratropical RCTT also corroborate a weakening of residual circulation cells in the extratropics of both hemispheres during El Niño. The pattern of changes in the residual circulation (transit time and stream function) depicts a weakening transition branch during El Niño, while the shallow branch is strengthening in both reanalyses. An ENSO-induced variability in the deep branch is less evident (not shown). In addition, the vertical structure of changes in the BD-circulation during El Niño, with a strengthening ascending branch and a weakening circulation in the midlatitudinal lower stratosphere, is also consistent with an upward shift of the strengthening shallow circulation branch and a weakening transition branch. The vertical structure of the BD-circulation branches agrees between the two reanalyses, although the changes in JRA-55 reanalysis are more confined in latitude and altitude than changes in ERA-I reanalysis, consistent with the variations in diabatic heating rates related to ENSO in the two reanalyses (Fig. 4(e, f)).

The most complete transit time diagnostic is the age spectrum, which includes the full transit time information related to all circulation pathways and mixing processes, thereby giving clearer insight into the reanalysis differences (discrepancies). From Figures 6(a–d), it can be concluded that the ENSO-induced variations in the age spectrum appear to be mainly caused by changes in the residual circulation and mass stream function (Fig. 5). Disentangling of the El Niño and La Niña impacts on the fraction of young air masses in the tropics and extratropics are consistent with the structural changes in the residual circulation induced by ENSO. Both reanalyses show an increase of the fraction of young air masses with age shorter than about 6 months during El Niño and significant decrease during La Niña in the tropical lower stratosphere (here 10°S–10°N at 400 K) (Fig. 6(a, b)). Note that JRA-55 depicts a smaller El Niño impact on the youngest air mass fraction than ERA-I, consistent with the reanalysis differences in the RCTTs (Fig. 5). The age spectrum tail, which is most sensitive to changes in mixing with very old air from the extratropics, is unchanged in both reanalyses after 25 months. Hence, the ENSO-induced changes in the tropical age spectrum mainly reflect the strengthening upwelling branch of the residual circulation in the tropics during El Niño, in agreement with the discussion by Konopka et al. (2016). In the midlatitudinal lower stratosphere (here 40°–55°N at 350 K), the age spectrum shows a decrease in the fraction of young air and a slight change in the spectrum tail after 40 months during

El Niño, indicating a long lasting ENSO signal in the northern hemisphere and mixing effect (Fig. 6 (c, d)). The amplitude of decreasing young air mass fraction during El Nino is larger in JRA-55 than in ERA-I, corroborating the observed differences in the AoA and RCTTs (Fig. 4 and 5). These changes in the age spectrum are consistent with the weakening transition branch of the residual circulation in the midlatitudinal lowermost stratosphere (see Fig. 5 and related discussion). Hence, the ENSO-induced changes in the lower stratospheric age spectra are consistent with the structural changes in the residual circulation, with El Niño causing an upward shift of the poleward outflow from the shallow branch of the BD-circulation and a weakening of the transition branch below. La Niña causes the opposite changes.

A very clear picture of the structural circulation changes induced by ENSO emerges from the separation of the young air mass fraction with transit time shorter than 6 months(Fig. 7(a, b)) and the old air mass fraction with transit time longer than 24 months (Fig. 7(c, d)), calculated from the age spectrum. During El Niño, the young air mass fraction with transit time shorter than 6 months increases throughout the tropical lower stratosphere and extends poleward in the layer between about 400–500 K. These changes in young air mass fraction are consistent with a strengthened shallow branch. In contrast, below about 400 K, the poleward transport of young tropical air weakens, and a negative young air anomaly even occurs during El Niño, consistent with the weakening transition branch and isolated midlatitudinal regions. Hence, El Niño clearly strengthens the shallow branch of the BD-circulation (above about 420 K) and weakens the transition branch, consistent in both reanalyses. The ENSO-induced variations in the air mass fraction with transit time longer than 24 months consistently show a significant decrease in the tropics and a significant increase in the extratropics in both reanalyses during El Niño (Fig. 7(c, d)). Differences between ERA-I and JRA-55 reanalyses are larger in the old air mass fractions, especially in the extratropics above 400 K, where JRA-55 exhibits larger positive anomalies in older air mass fraction than ERA-I. The signal of the old air mass fraction with transit time longer than 24 months from JRA-55 spreads throughout the lower stratosphere except in the tropics. Despite the differences in the distribution of the old air mass fraction between ERA-I and JRA-55 reanalyses, the decrease of old air in the tropics and the increase of old air in the extratropics is consistent between the two reanalyses. Note that the ENSO-induced changes are less evident above about 600 K (not shown), indicating that the ENSO impact on the BD-circulation is largely confined to the region below and hence to the transition and shallow branches.

5 Discussion

In a recent study, Yang et al. (2014) showed from an idealized model that zonally symmetric SST perturbations drive the deep branch of the stratospheric BD-circulation, whereas zonally localized SST perturbations drive the shallow circulation branch. Here, we find no clear evidence for an El Niño effect on the deep branch of the BD-circulation above about 600 K. Nevertheless, our results are consistent with the findings of Yang et al. (2014), who suggested that a zonally symmetric anomalous SST pattern suppress the isentropic mixing induced by a stronger subtropical jet. We also found that El Niño alters both sub-branches of the BD-circulation i.e., strengthens the shallow branch and weakens the transition branch. Hence, El Niño shifts the shallow circulation branch upwards and weakens the transition branch between about 370–420 K.

Atmos. Chem. Phys. Discuss., https://doi.org/10.5194/acp-2018-688
Manuscript under review for journal Atmos. Chem. Phys.
Discussion started: 6 August 2018

Atmospheric Chemistry and Physics Discussions

Insight into the underlying dynamical mechanism causing the changes in the transition and shallow branches of the BD-circulation is derived from the temperature, zonal mean wind and Eliassen-Palm flux (EP-flux) divergence variations related to ENSO (Fig. 8). Generally both reanalyses agree well in ENSO-induced variations in temperature, zonal mean wind and EP-flux divergence anomalies. In the tropics (30° S–30° N), El Niño clearly warms the upper troposphere and cools the lower stratosphere, consistent with previous studies (e.g., Randel et al., 2009; Calvo et al., 2010; Simpson et al., 2011). Large tropical temperature changes remain confined below about 500 K. In the extratropics, El Niño generally warms the whole lower stratosphere, except below about 400 K near the subtropical jets, where negative temperature anomalies occur (Fig. 8(a, d)). The cooling of the tropical stratosphere and warming of the extratropical lower stratosphere are consistent with the increased tropical upwelling and extratropical downwelling during El Niño. In addition, the negative temperature anomalies in the mid-latitudes are consistent with a weakening transition branch. The strong differences in the temperature changes between the upper tropical troposphere and the midlatitudes (i.e. strong tropical-midlatitudinal temperature gradient) cause a strengthening of the subtropical and polar zonal jets on their equatorward flanks, resulting in an equatorward and an upward shift of the subtropical jet (∼10° and ∼10 K) (Fig. 8(b, e)), consistent with the results of Lorenz and DeWeaver (2007). According to Simpson et al. (2011), this equatorward shift of the mid-latitude jet related to El Niño results in an enhanced source of waves of higher phase speeds in the midlatitudes in changed propagation characteristics into the stratosphere. Recently, Albers et al. (2018) also attributed the ENSO-related jet variability to wave breaking frequency rather than to the typical ENSO teleconnection patterns. The temperature and zonal mean wind variations induced by El Niño agree with prior model and observational studies (e.g., Lu et al., 2008; Simpson et al., 2011; Abalos et al., 2017; Zhou et al., 2018) and with the idealized model results from Yang et al. (2014). This ENSO-induced variability in temperatures and zonal wind can be understood as a direct response to the zonal extent of the SST perturbations. The changes in EP-flux divergence related to El Niño show positive anomalies at lower levels close to the tropopause and negative anomalies in the midlatitudinal lower stratosphere above about 420 K (Fig. 8(c, f)). The positive anomalies suggest decreased planetary Rossby and gravity wave breaking at lower levels in the lower stratosphere during El Niño (McLandress and Shepherd, 2009; Calvo et al., 2010; Simpson et al., 2011), consistent with the weakening of the transition branch. In contrast, the negative anomalies indicate that more waves break at higher levels in the extratropical lower stratosphere, depositing their momentum flux in these regions, and therefore accelerating the shallow branch (Fig. 8(c, f)). Hence, the wave driving changes shown in Fig. 8(c, f) are qualitatively consistent with a weakening of the transition branch of the BD-circulation and a strengthening of the shallow branch during El Niño. These wave driving changes are also consistent with the findings of Zhou et al. (2018), who concluded that the magnitudes of the stratospheric zonal mean responses are larger in the case of extreme El Niño events, as the strong upward propagation of planetary-scale waves induces a weaker northern hemisphere polar vortex by breaking at high-latitudes.

Gravity waves have been shown to play an important role in driving ENSO related variations in the lower stratospheric circulation, particularly in the subtropics (Calvo et al., 2010; Simpson et al., 2011). According to Alexander et al. (2017), zonal gravity wave momentum fluxes at the tropopause were 11 % smaller during El Niño than during La Niña because of a shift in the precipitation to the central Pacific, where upper tropospheric zonal winds are less favorable for vertical wave propagation. According to Kawatani et al. (2010), zonal mean variation of wave forcings in the stratosphere results from the

Atmos. Chem. Phys. Discuss., https://doi.org/10.5194/acp-2018-688
Manuscript under review for journal Atmos. Chem. Phys.
Discussion started: 6 August 2018

Atmospheric Chemistry and Physics Discussions

phase of the QBO and the changes in wave sources, i.e. the vertically shear of zonal mean winds associated with the Walker circulation. Hence, close agreement between the ENSO variations in the wave driving and the residual circulation variations is not necessarily expected, due to the strong effect of gravity waves.

Future projections of climate models predict a shift of the ENSO basic state toward more frequent El Niño conditions in a warming climate due to increasing in anthropogenic greenhouse gases (Timmermann et al., 1999; van Oldenborgh et al., 2005; Latif and Keenlyside, 2009; Cai et al., 2014). As changes in UTLS trace gases, including O_3 and H_2O (Solomon et al., 2010; Riese et al., 2012), directly impact the global radiative forcing of climate (Forster and Shine, 1999; Butchart and Scaife, 2001), it is crucial to understand such future changes in trace gases induced by a shift of the ENSO basic state toward more frequent El Niño-like conditions. Despite the uncertainty in the magnitude of the future El Niño events, we speculate that the projected change in the El Niño occurrence frequency will cause structural changes similar to the current O_3, RCTT and $\dot{\theta}$ anomalies (Fig. 3, 4 and 5). In a future climate characterised by a shift of the basic state toward more frequent El Niño conditions, the negative O_3 anomalies in the tropics and positive O_3 anomalies in the midlatitudes will strengthen, (by at least 15 %), inducing enhanced stratosphere-to-troposphere exchanges of ozone mass flux (Holton et al., 1995; Hegglin and Shepherd, 2009; Neu et al., 2014; Yang et al., 2016; Albers et al., 2018; Meul et al., 2018) and stronger ozone radiative feedback (Forster and Shine, 1997; Birner and Charlesworth, 2017; Ming et al., 2017).

6 Summary and Conclusions

Based on an established multiple regression method applied to MLS observations and CLaMS simulations driven by ERA-I and JRA-55 reanalysis, we found that ENSO induces structural changes of the BD-circulation in the lower stratosphere. These structural changes in the BD-circulation lead to substantial changes in the tropical and midlatitudinal lower stratospheric O_3 anomalies of about 15 % for MLS observations.

The regression analysis of different metrics of the circulation strength related to ENSO, including mean AoA, $\overline{w^*}$, RCTT, ψ^* and age spectra, shows structural changes in the lower stratospheric BD-circulation branches, consistent with observed O_3 anomalies. The ENSO influence on the BD-circulation turns out to be mainly evident for the transition and shallow circulation branches (Birner and Bönisch, 2011; Lin and Fu, 2013). During El Niño, the transition branch weakens, while the shallow branch strengthens. These structural changes in the transition and shallow branches are tightly linked to the dynamical response of the atmosphere to ENSO. During El Niño, the strengthened tropical-midlatitudinal temperature gradient induces a strengthening of the subtropical zonal jets on their equatorward flanks, resulting in an equatorward and upward shift of the subtropical jet. This equatorward shift of the mid-latitude jet induced by El Niño results in an enhanced wave propagation towards the extratropical lower stratosphere and breaking therein, consistent with the structural changes in the BD-circulation. During La Niña, an opposite changes occur (not shown).

These structural circulation changes related to ENSO affect the distributions of radiatively active trace gases, including O_3, in the UTLS which, in turn, crucially impact the global radiation budget (Forster and Shine, 1999; Butchart and Scaife, 2001). Hence, the ENSO influence on the structure of the BD-circulation in the UTLS opens a pathway for a stratospheric impact on

future climate. Our results suggest that in the context of a changing future climate, where increasing El Niño-like conditions (Timmermann et al., 1999; Cai et al., 2014) and decreasing lower stratospheric QBO amplitude (Kawatani and Hamilton, 2013) are expected, the ENSO effect will be increasingly important for controlling the distributions of radiatively active greenhouse gases in the UTLS.

Data availability. Aura Microwave Limb Sounder product (https://mls.jpl.nasa.gov/) and ERA-Interim reanalysis data (https://www.ecmwf.int/en/forecasts/datasets/reanalysis-datasets/era-interim). CLaMS O_3, AoA, $\overline{w^*}$, RCTT and age spectrum data set can be requested from the corresponding author F. Ploeger (f.ploeger@fz-juelich.de).

Competing interests. The authors declare that they have no conflict of interest.

Acknowledgements. We particularly thank the NASA Jet Propulsion Laboratory, the European Centre for Medium-Range Weather Forecasts and Japan Meteorological Agency for providing Aura Microwave Limb Sounder product (https://mls.jpl.nasa.gov/), the ERA-Interim and JRA-55 reanalyses data. Work at the Jet Propulsion Laboratory, California Institute of Technology, was done under contract with the National Aeronautics and Space Administration. This work was funded by the Helmholtz Association under grant number VH-NG-1128 (Helmholtz-Hochschul-Nachwuchsforschergruppe), a research stay at the Institute of Energy and Climate Research, Stratosphere (IEK-7), Forschungszentrum in Jülich during which this work had been carried out.

References

Abalos, M., Legras, B., Ploeger, F., and Randel, W. J.: Evaluating the advective Brewer-Dobson circulation in three reanalyses for the period 1979–2012, J. Geophys. Res. Atmos., 120, 7534–7554, https://doi.org/10.1002/2015JD023182, 2015.

Abalos, M., Randel, W. J., Kinnison, D. E., and Garcia, R. R.: Using the Artificial Tracer e90 to Examine Present and Future UTLS Tracer Transport in WACCM, J. Atmos. Sci., 74, 3383–3403, https://doi.org/10.1175/JAS-D-17-0135.1, https://doi.org/10.1175/JAS-D-17-0135.1, 2017.

Albers, J. R., Perlwitz, J., Butler, A. H., Birner, T., Kiladis, G. N., Lawrence, Z. D., Manney, G. L., Langford, A. O., and Dias, J.: Mechanisms Governing Interannual Variability of Stratosphere to Troposphere Ozone Transport, J. Geophys. Res.: Atmos., 123, 234–260, https://doi.org/10.1002/2017JD026890, https://agupubs.onlinelibrary.wiley.com/doi/abs/10.1002/2017JD026890, 2018.

Alexander, M. J., Ortland, D. A., Grimsdell, A. W., and Kim, J.-E.: Sensitivity of Gravity Wave Fluxes to Interannual Variations in Tropical Convection and Zonal Wind, J. Atmos. Sci., 74, 2701–2716, https://doi.org/10.1175/JAS-D-17-0044.1, https://doi.org/10.1175/JAS-D-17-0044.1, 2017.

Andrews, D. G., Holton, J. R., and Leovy, C. B.: Middle Atmosphere Dynamics, vol. 40 of *Int. Geophys. Series*, Academic Press, San Diego, USA, 1987.

Avery, M. A., Davis, S. M., Rosenlof, K. H., Ye, H., and Dessler, A. E.: Large anomalies in lower stratospheric water vapour and ice during the 2015–2016 El Niño, Nat. Geosci., https://doi.org/10.1038/ngeo2961, 2017.

Baldwin, M. P. and O'Sullivan, D.: Stratospheric Effects of ENSO-Related Tropospheric Circulation Anomalies, J. of Clim., 8, 649–667, https://doi.org/10.1175/1520-0442(1995)008<0649:SEOERT>2.0.CO;2, https://doi.org/10.1175/1520-0442(1995)008<0649:SEOERT>2.0.CO;2, 1995.

Bence, J. R.: Analysis of short time series: Correcting for autocorrelation, Ecology, 76, pp. 628–639, http://www.jstor.org/stable/1941218, 1995.

Birner, T. and Bönisch, H. B.: Residual circulation trajectories and transit times into the extratropical lowermost stratosphere, Atmos. Chem. Phys., 11, 817–827, https://doi.org/10.5194/acp-11-817-2011, 2011.

Birner, T. and Charlesworth, E. J.: On the relative importance of radiative and dynamical heating for tropical tropopause temperatures, J. Geophys. Res., 122, 6782–6797, https://doi.org/10.1002/2016JD026445, http://dx.doi.org/10.1002/2016JD026445, 2016JD026445, 2017.

Bjerknes, J.: Atmospheric teleconnections from the equatorial Pacific, Monthly Weather Rev., 97, 163–172, https://doi.org/10.1175/1520-0493(1969)097<0163:ATFTEP>2.3.CO;2, https://doi.org/10.1175/1520-0493(1969)097$<$0163:ATFTEP$>$2.3.CO;2, 1969.

Bönisch, H. B., Engel, A., Birner, T., Hoor, P., Tarasick, D. W., and Ray, E. A.: On the structural changes in the Brewer-Dobson circulation after 2000, Atmos. Chem. Phys., 11, 3937–3948, https://doi.org/10.5194/acp-11-3937-2011, 2011.

Brewer, A.: Evidence for a world circulation provided by the measurements of helium and water vapour distribution in the stratosphere, Q. J. R. Meteorol. Soc., 75, 351–363, 1949.

Brönnimann, S., Xoplaki, E., Casty, C., Pauling, A., and Luterbacher, J.: ENSO influence on Europe during the last centuries, Clim. Dyn., 28, 181–197, https://doi.org/10.1007/s00382-006-0175-z, http://dx.doi.org/10.1007/s00382-006-0175-z, 2007.

Butchart, N.: The Brewer-Dobson circulation, Rev. Geophys., 52, 157–184, https://doi.org/10.1002/2013RG000448, http://dx.doi.org/10.1002/2013RG000448, 2014.

Butchart, N. and Scaife, A. A.: Removal of chlorofluorocarbons by increased mass exchange between the stratosphere and troposphere in a changing climate., Nature, 410, 799–802, https://doi.org/10.1038/35071047, 2001.

Butler, A. H., Polvani, L. M., and Deser, C.: Separating the stratospheric and tropospheric pathways of El Nino-Southern Oscillation teleconnections, Envir. Res. Lett., 9, 024 014, http://stacks.iop.org/1748-9326/9/i=2/a=024014, 2014.

Cagnazzo, C. and Manzini, E.: Impact of the Stratosphere on the Winter Tropospheric Teleconnections between ENSO and the North Atlantic and European Region, J. of Clim., 22, 1223–1238, https://doi.org/10.1175/2008JCLI2549.1, https://doi.org/10.1175/2008JCLI2549.1, 2009.

Cai, W., Borlace, S., Lengaigne, M., van Rensch, P., Collins, M., Vecchi, G., Timmermann, A., Santoso, A., McPhaden, M. J., Wu, L., England, M. H., Wang, G., Guilyardi, E., and Jin, F.-F.: Increasing frequency of extreme El Niño events due to greenhouse warming, Nat. Clim. Change, 4, 111–116, https://doi.org/10.1038/nclimate2100, http://dx.doi.org/10.1038/nclimate2100, 2014.

Calvo, N., García-Herrera, R., and Garcia, R. R.: The ENSO Signal in the Stratosphere, Annals of the New York Acad. of Sci., 1146, 16–31, https://doi.org/10.1196/annals.1446.008, http://dx.doi.org/10.1196/annals.1446.008, 2008.

Calvo, N., Garcia, R. R., Randel, W. J., and Marsh, D. R.: Dynamical mechanism for the increase in tropical upwelling in the lowermost tropical stratosphere during warm ENSO events, J. Atmos. Sci., 67, 2331–2340, https://doi.org/10.1175/2010JAS3433.1, 2010.

Calvo-Fernandez, N., Garcia-Herrera, R., Gallego-Puyol, D., Hernandez-Martin, E., Garcia, R. R., Gimeno-Presa, L., and Ribera-Rodriguez, P.: Analysis of the ENSO Signal in Tropospheric and Stratospheric Temperatures Observed by MSU, 1979-2000, J. Clim., 17, 3934–3946, https://doi.org/10.1175/1520-0442(2004)017<3934:AOTESI>2.0.CO;2, 2004.

Chandra, S., Ziemke, J. R., Schoeberl, M. R., Froidevaux, L., Read, W. G., Levelt, P. F., and Bhartia, P. K.: Effects of the 2004 El Niño on tropospheric ozone and water vapor, Geophys. Res. Lett., 34, https://doi.org/10.1029/2006GL028779, https://agupubs.onlinelibrary.wiley.com/doi/abs/10.1029/2006GL028779, 2007.

Chandra, S., Ziemke, J. R., Duncan, B. N., Diehl, T. L., Livesey, N. J., and Froidevaux, L.: Effects of the 2006 El Niño on tropospheric ozone and carbon monoxide: implications for dynamics and biomass burning, Atmos. Chem. Phys., 9, 4239–4249, https://doi.org/10.5194/acp-9-4239-2009, https://www.atmos-chem-phys.net/9/4239/2009/, 2009.

Dee, D. P., Uppala, S. M., Simmons, A. J., Berrisford, P., Poli, P., Kobayashi, S., Andrae, U., Balmaseda, M. A., Balsamo, G., Bauer, P., Bechtold, P., Beljaars, A. C. M., van de Berg, L., Bidlot, J., Bormann, N., Delsol, C., Dragani, R., Fuentes, M., Geer, A. J., Haimberger, L., Healy, S. B., Hersbach, H., Hólm, E. V., Isaksen, L., Kållberg, P., Köhler, M., Matricardi, M., McNally, A. P., Monge-Sanz, B. M., Morcrette, J.-J., Park, B.-K., Peubey, C., de Rosnay, P., Tavolato, C., Thépaut, J.-N., and Vitart, F.: The ERA-Interim reanalysis: configuration and performance of the data assimilation system, Q. J. R. Meteorol. Soc., 137, 553–597, https://doi.org/10.1002/qj.828, 2011.

Dessler, A. E., Schoeberl, M. R., Wang, T., Davis, S. M., and Rosenlof, K. H.: Stratospheric water vapor feedback, Proceed. Nat. Acad. Sci., 110 45, 18 087–91, 2013.

Diallo, M., Legras, B., and Chédin, A.: Age of stratospheric air in the ERA-Interim, Atmos. Chem. Phys., 12, 12 133–12 154, https://doi.org/10.5194/acp-12-12133-2012, 2012.

Diallo, M., Ploeger, F., Konopka, P., Birner, T., Müller, R., Riese, M., Garny, H., Legras, B., Ray, E., Berthet, G., and Jegou, F.: Significant contributions of volcanic aerosols to decadal changes in the stratospheric circulation, Geophys. Res. Lett., https://doi.org/10.1002/2017GL074662, http://dx.doi.org/10.1002/2017GL074662, 2017.

Diallo, M., Riese, M., Birner, T., Konopka, P., Müller, R., Hegglin, M. I., Santee, M. L., Baldwin, M., Legras, B., and Ploeger, F.: Response of stratospheric water vapor and ozone to the unusual timing of El Niño and QBO disruption in 2015–2016, Atmos. Chem. and Phys. Discus., 2018, 1–26, https://doi.org/10.5194/acp-2018-239, https://www.atmos-chem-phys-discuss.net/acp-2018-239/, 2018.

Field, R. D., van der Werf, G. R., Fanin, T., Fetzer, E. J., Fuller, R., Jethva, H., Levy, R., Livesey, N. J., Luo, M., Torres, O., and Worden, H. M.: Indonesian fire activity and smoke pollution in 2015 show persistent nonlinear sensitivity to El Niño-induced drought, Proceed. Nat. Acad. Sci., https://doi.org/10.1073/pnas.1524888113, http://www.pnas.org/content/early/2016/07/27/1524888113, 2016.

Forster, P. M. and Shine, K. P.: Stratospheric water vapour changes as a possible contributor to observed stratospheric cooling, Geophys. Res. Lett., 26, 3309–3312, https://doi.org/10.1029/1999GL010487, http://dx.doi.org/10.1029/1999GL010487, 1999.

Forster, P. M. D. F. and Shine, K. P.: Radiative forcing and temperature trends from stratospheric ozone changes, Geophys. Res. Lett., 102, 10 841–10 855, https://doi.org/10.1029/96JD03510, 1997.

Forster, P. M. d. F. and Shine, K. P.: Assessing the climate impact of trends in stratospheric water vapor, Geophys. Res. Lett., 29, https://doi.org/10.1029/2001GL013909, http://dx.doi.org/10.1029/2001GL013909, 2002.

Froidevaux, L., Jiang, Y. B., Lambert, A., Livesey, N. J., Read, W. G., Waters, J. W., Browell, E. V., Hair, J. W., Avery, M. A., McGee, T. J., Twigg, L. W., Sumnicht, G. K., Jucks, K. W., Margitan, J. J., Sen, B., Stachnik, R. A., Toon, G. C., Bernath, P. F., Boone, C. D., Walker, K. A., Filipiak, M. J., Harwood, R. S., Fuller, R. A., Manney, G. L., Schwartz, M. J., Daffer, W. H., Drouin, B. J., Cofield, R. E., Cuddy, D. T., Jarnot, R. F., Knosp, B. W., Perun, V. S., Snyder, W. V., Stek, P. C., Thurstans, R. P., and Wagner, P. A.: Validation of Aura Microwave Limb Sounder stratospheric ozone measurements, J. Geophys. Res.: Atmos., 113, https://doi.org/10.1029/2007JD008771, http://dx.doi.org/10.1029/2007JD008771, 2008.

Fromm, M., Tupper, A., Rosenfeld, D., Servranckx, R., and McRae, R.: Violent pyro-convective storm devastates Australia's capital and pollutes the stratosphere, Geophys. Res. Lett., 33, https://doi.org/10.1029/2005GL025161, 2006.

Fromm, M. D. and Servranckx, R.: Transport of forest fire smoke above the tropopause by supercell convection, Geophys. Res. Lett., 30, https://doi.org/10.1029/2002GL016820, 2003.

Fueglistaler, S., Dessler, A. E., Dunkerton, T. J., Folkins, I., Fu, Q., and Mote, P. W.: Tropical Tropopause Layer, Rev. Geophys., 47, G1004+, https://doi.org/10.1029/2008RG000267, 2009a.

Fueglistaler, S., Legras, B., Beljaars, A., Morcrette, J.-J., Simmons, A., Tompkins, A. M., and Uppala, S.: The diabatic heat budget of the upper troposphere and lower/mid stratosphere in ECMWF reanalyses, Q. J. R. Meteorol. Soc., 135, 21–37, https://doi.org/10.1002/qj.361, http://dx.doi.org/10.1002/qj.361, 2009b.

Fujiwara, M., Wright, J. S., Manney, G. L., Gray, L. J., Anstey, J., Birner, T., Davis, S., Gerber, E. P., Harvey, V. L., Hegglin, M. I., Homeyer, C. R., Knox, J. A., Krüger, K., Lambert, A., Long, C. S., Martineau, P., Molod, A., Monge-Sanz, B. M., Santee, M. L., Tegtmeier, S., Chabrillat, S., Tan, D. G. H., Jackson, D. R., Polavarapu, S., Compo, G. P., Dragani, R., Ebisuzaki, W., Harada, Y., Kobayashi, C., McCarty, W., Onogi, K., Pawson, S., Simmons, A., Wargan, K., Whitaker, J. S., and Zou, C.-Z.: Introduction to the SPARC Reanalysis Intercomparison Project (S-RIP) and overview of the reanalysis systems, Atmos. Chem. Phys., 17, 1417–1452, https://doi.org/10.5194/acp-17-1417-2017, https://www.atmos-chem-phys.net/17/1417/2017/, 2017.

Garcia-Herrera, R., Calvo, N., Garcia, R. R., and Giorgetta, M. A.: Propagation of ENSO temperature signals into the middle atmosphere: A comparison of two general circulation models and ERA-40 reanalysis data, J. Geophys. Res.: Atmos., 111, https://doi.org/10.1029/2005JD006061, https://agupubs.onlinelibrary.wiley.com/doi/abs/10.1029/2005JD006061, 2006.

Garfinkel, C. I. and Hartmann, D. L.: Effects of the El Niño–Southern Oscillation and the Quasi-Biennial Oscillation on polar temperatures in the stratosphere, J. Geophys. Res.: Atmos., 112, https://doi.org/10.1029/2007JD008481, http://dx.doi.org/10.1029/2007JD008481, 2007.

Garfinkel, C. I. and Hartmann, D. L.: Different ENSO teleconnections and their effects on the stratospheric polar vortex, J. Geophys. Res.: Atmos., 113, https://doi.org/10.1029/2008JD009920, http://dx.doi.org/10.1029/2008JD009920, 2008.

Garny, H., Birner, T., Bönisch, H., and Bunzel, F.: The effects of mixing on age of air, J. Geophys. Res. Atmos., 119, https://doi.org/10.1002/2013JD021417, 2014.

Hall, T. and Plumb, R. A.: Age as a diagnostic of stratospheric transport, J. Geophys. Res., 99, 1059–1070, 1994.

Haynes, P. H., McIntyre, M. E., Shepherd, T. G., Marks, C. J., and Shine, K. P.: On the "Downward Control" of Extratropical Diabatic Circulations by Eddy-Induced Mean Zonal Forces, J. Atmos. Sci., 48, 651–678, https://doi.org/10.1175/1520-0469(1991)048<0651:OTCOED>2.0.CO;2, https://doi.org/10.1175/1520-0469(1991)048$<$0651:OTCOED$>$2.0.CO;2, 1991.

Hegglin, M. I. and Shepherd, T. G.: Large climate–induced changes in ultraviolet index and stratosphere–to–troposphere ozone flux, Nat. Geosci., 2, 687–691, https://doi.org/10.1038/ngeo604, http://dx.doi.org/10.1038/ngeo604, 2009.

Holton, J. R., Haynes, P. H., McIntyre, M. E., Douglass, A. R., Rood, R. B., and Pfister, L.: Stratosphere–troposphere exchange, Rev. Geophys., 33, 403–440, https://doi.org/10.1029/95RG02097, 1995.

Ineson, S. and Scaife, A. A.: The role of the stratosphere in the European climate response to El Niño, Nat. Geosci., 2, 32–36, https://doi.org/10.1038/ngeo381, 2009.

Kawatani, Y. and Hamilton, K.: Weakened stratospheric quasibiennial oscillation driven by increased tropical mean upwelling, Nature, 497, 478–481, https://doi.org/doi:10.1038/nature12140, http://dx.doi.org/10.1038/nature12140, 2013.

Kawatani, Y., Watanabe, S., Sato, K., Dunkerton, T. J., Miyahara, S., and Takahashi, M.: The Roles of Equatorial Trapped Waves and Internal Inertia–Gravity Waves in Driving the Quasi-Biennial Oscillation. Part I: Zonal Mean Wave Forcing, J. Atmos. Sci., 67, 963–980, https://doi.org/10.1175/2009JAS3222.1, https://doi.org/10.1175/2009JAS3222.1, 2010.

Khaykin, S. M., Godin-Beekmann, S., Keckhut, P., Hauchecorne, A., Jumelet, J., Vernier, J.-P., Bourassa, A., Degenstein, D. A., Rieger, L. A., Bingen, C., Vanhellemont, F., Robert, C., DeLand, M., and Bhartia, P. K.: Variability and evolution of the midlatitude stratospheric aerosol budget from 22 years of ground-based lidar and satellite observations, Atmos. Chem. Phys., 17, 1829–1845, https://doi.org/10.5194/acp-17-1829-2017, https://www.atmos-chem-phys.net/17/1829/2017/, 2017.

Kobayashi, S., Ota, Y., Harada, Y., Ebita, A., Boriya, M., Onoda, H., Onogi, K., Kamahori, H., Endo, H., Miyaoka, K., and Takahashi, K.: The JRA-55 Reanalysis: General Specifications and Basic Characteristics, J. of the Meteo. Soc. of Japan, 93, 5–48, https://doi.org/10.2151/jmsj.2015-001, 2015.

Konopka, P., Steinhorst, H.-M., Grooß, J.-U., Günther, G., Müller, R., Elkins, J., Jost, H.-J., Richard, E., Schmidt, U., Toon, G., and McKenna, D.: Mixing and ozone loss in the 1999-2000 Arctic vortex: simulations with the three-dimensional Chemical Lagrangian Model of the Stratosphere (CLaMS), J. Geophys. Res., 109(D2), 2315, https://doi.org/10.1029/2003JD003792, 2004.

Konopka, P., Ploeger, F., Tao, M., and Riese, M.: Zonally resolved impact of ENSO on the stratospheric circulation and water vapor entry values, J. Geophys. Res.: Atmos., 121, 11,486–11,501, https://doi.org/10.1002/2015JD024698, http://dx.doi.org/10.1002/2015JD024698, 2016.

Latif, M. and Keenlyside, N. S.: El Niño/Southern Oscillation response to global warming, Proceed. of the Nat. Acad. of Sci., 106, 20 578–20 583, https://doi.org/10.1073/pnas.0710860105, http://www.pnas.org/content/106/49/20578.abstract, 2009.

L'Heureux, M. L., Takahashi, K., Watkins, A. B., Barnston, A. G., Becker, E. J., Liberto, T. E. D., Gamble, F., Gottschalck, J., Halpert, M. S., Huang, B., Mosquera-Vásquez, K., and Wittenberg, A. T.: Observing and Predicting the 2015/16 El Niño, Bulletin of the American Meteor. Soc., 98, 1363–1382, https://doi.org/10.1175/BAMS-D-16-0009.1, https://doi.org/10.1175/BAMS-D-16-0009.1, 2017.

Li, F., Waugh, D. W., Douglass, A. R., Newman, P. A., Pawson, S., Stolarski, R. S., Strahan, S. E., and Nielsen, J. E.: Seasonal variations of stratospheric age spectra in the Goddard Earth Observing System Chemistry Climate Model (GEOSCCM), J. Geophys. Res., 117, 134, https://doi.org/10.1029/2011JD016877, 2012.

Liess, S. and Geller, M. A.: On the relationship between QBO and distribution of tropical deep convection, J. Geophys. Res.: Atmos., 117, https://doi.org/10.1029/2011JD016317, http://dx.doi.org/10.1029/2011JD016317, 2012.

Lin, P. and Fu, Q.: Changes in various branches of the Brewer–Dobson circulation from an ensemble of chemistry climate models, J. Geophys. Res.: Atmos., 118, 73–84, https://doi.org/10.1029/2012JD018813, http://dx.doi.org/10.1029/2012JD018813, 2013.

Livesey, N. J., Filipiak, M. J., Froidevaux, L., Read, W. G., Lambert, A., Santee, M. L., Jiang, J. H., Pumphrey, H. C., Waters, J. W., Cofield, R. E., Cuddy, D. T., Daffer, W. H., Drouin, B. J., Fuller, R. A., Jarnot, R. F., Jiang, Y. B., Knosp, B. W., Li, Q. B., Perun, V. S., Schwartz, M. J., Snyder, W. V., Stek, P. C., Thurstans, R. P., Wagner, P. A., Avery, M., Browell, E. V., Cammas, J.-P., Christensen, L. E., Diskin, G. S., Gao, R.-S., Jost, H.-J., Loewenstein, M., Lopez, J. D., Nedelec, P., Osterman, G. B., Sachse, G. W., and Webster, C. R.: Validation of Aura Microwave Limb Sounder O3 and CO observations in the upper troposphere and lower stratosphere, J. Geophys. Res., 113, 10 195–10 213, https://doi.org/10.1029/2007JD008805, 2008.

Livesey, N. J., Read, W. G., Froidevaux, L. Lambert, A., Manney, G. L., Pumphrey, H. C., Santee, M. L., Schwartz, M. J., Wang, S., Cofield, R. E., Cuddy, D. T., Fuller, R. A., Jarnot, R. F., Jiang, J. H., Knosp, B. W., Stek, P. C., Wagner, P. A., and Wu, D. L.: EOS MLS Version 3.3 and 3.4 Level 2 data quality and description document, Tech. Rep., JPL JPL D-33509 Rev. C, pp. 1–162, availableat:http://mls.jpl.nasa.gov/, 2013.

Livesey, N. J., Read, W. G., Wagner, P. A., Froidevaux, L., Lambert, A., Manney, G. L., Millán Valle, L. F., Pumphrey, H. C., Santee, M. L., Schwartz, M. J., Wang, S., Fuller, R. A., Jarnot, R. F., Knosp, B. W., and Martinez, E.: Aura Microwave Limb Sounder (MLS) Version 4.2x Level 2 data quality and description document, Tech. Rep. JPL D-33509 Rev. C, pp. 1–169, https://doi.org/10.5194/acp-15-9945-2015, availableat:http://mls.jpl.nasa.gov/, 2017.

Logan, J. A., Megretskaia, I., Nassar, R., Murray, L. T., Zhang, L., Bowman, K. W., Worden, H. M., and Luo, M.: Effects of the 2006 El Niño on tropospheric composition as revealed by data from the Tropospheric Emission Spectrometer (TES), Geophys. Res. Lett., 35, https://doi.org/10.1029/2007GL031698, https://agupubs.onlinelibrary.wiley.com/doi/abs/10.1029/2007GL031698, 2008.

Lorenz, D. J. and DeWeaver, E. T.: Tropopause height and zonal wind response to global warming in the IPCC scenario integrations, J. Geophys. Res., 112, https://doi.org/10.1029/2006JD008087, http://dx.doi.org/10.1029/2006JD008087, 2007.

Lu, J., Chen, G., and Frierson, D. M. W.: Response of the Zonal Mean Atmospheric Circulation to El Niño versus Global Warming, J. of Clim., 21, 5835–5851, https://doi.org/10.1175/2008JCLI2200.1, https://doi.org/10.1175/2008JCLI2200.1, 2008.

Manzini, E., Giorgetta, M. A., Esch, M., Kornblueh, L., and Roeckner, E.: The Influence of Sea Surface Temperatures on the Northern Winter Stratosphere: Ensemble Simulations with the MAECHAM5 Model, J. of Clim., 19, 3863–3881, https://doi.org/10.1175/JCLI3826.1, https://doi.org/10.1175/JCLI3826.1, 2006.

McKenna, D., Konopka, P., Grooß, J.-U., Günther, G., Müller, R., Spang, R., Offermann, D., and Orsolini, Y.: A new Chemical Lagrangian Model of the Stratosphere (CLaMS): 1. Formulation of advection and mixing, J. Geophys. Res., 107, 4309, doi:10.029/2000JD000 114, 2002.

McLandress, C. and Shepherd, T. G.: Simulated anthropogenic changes in the Brewer-Dobson Circulation, Including Its Extension to High Latitudes, J. of Clim., 22, 1516, https://doi.org/10.1175/2008JCLI2679.1, 2009.

Meul, S., Langematz, U., Kröger, P., Oberländer-Hayn, S., and Jöckel, P.: Future changes in the stratosphere to troposphere ozone mass flux and the contribution from climate change and ozone recovery, Atmos. Chem. Phys., 18, 7721–7738, https://doi.org/10.5194/acp-18-7721-2018, https://www.atmos-chem-phys.net/18/7721/2018/, 2018.

Ming, A., Maycock, A. C., Hitchcock, P., and Haynes, P.: The radiative role of ozone and water vapour in the annual temperature cycle in the tropical tropopause layer, Atmos. Chem. Phys., 17, 5677–5701, https://doi.org/10.5194/acp-17-5677-2017, https://www.atmos-chem-phys.net/17/5677/2017/, 2017.

Nassar, R., Logan, J. A., Megretskaia, I. A., Murray, L. T., Zhang, L., and Jones, D. B. A.: Analysis of tropical tropospheric ozone, carbon monoxide, and water vapor during the 2006 El Niño using TES observations and the GEOS Chem model, J. Geophys. Res.: Atmos., 114, https://doi.org/10.1029/2009JD011760, https://agupubs.onlinelibrary.wiley.com/doi/abs/10.1029/2009JD011760, 2009.

Neu, J. L., Flury, T., Manney, G. L., Santee, M. L., Livesey, N. J., and Worden, J.: Tropospheric ozone variations governed by changes in stratospheric circulation, Nat. Geosci., 7, 340–344, https://doi.org/10.1038/ngeo2138, http://dx.doi.org/10.1038/355626a0, 2014.

Newman, P. A. and Nash, E. R.: Quantifying the wave driving of the stratosphere, J. Geophys. Res.: Atmos., 105, 12 485–12 497, https://doi.org/10.1029/1999JD901191, http://dx.doi.org/10.1029/1999JD901191, 2000.

Niwano, M., Yamazaki, K., and Shiotani, M.: Seasonal and QBO variations of ascent rate in the tropical lower stratosphere as inferred from UARS HALOE trace gas data, J. Geophys. Res., 108, 4794, https://doi.org/10.1029/2003JD003871, http://dx.doi.org/10.1029/2003JD003871, 4794, 2003.

Philander, S. G.: El Niño, La Nina, and the Southern Oscillation, vol. 46 of *Academic Press*, Cambridge Univ. Press, San Diego, CA, 1990.

Ploeger, F. and Birner, T.: Seasonal and inter-annual variability of lower stratospheric age of air spectra, Atmos. Chem. Phys., 16, 10 195–10 213, https://doi.org/10.5194/acp-16-10195-2016, http://www.atmos-chem-phys.net/16/10195/2016/, 2016.

Ploeger, F., Abalos, M., Birner, T., Konopka, P., Legras, B., Müller, R., and Riese, M.: Quantifying the effects of mixing and residual circulation on trends of stratospheric mean age of air, Geophys. Res. Lett., 42, https://doi.org/10.1002/2014GL062927, 2015a.

Ploeger, F., Riese, M., Haenel, F., Konopka, P., Müller, R., and Stiller, G.: Variability of stratospheric mean age of air and of the local effects of residual circulation and eddy mixing, J. Geophys. Res. Atmos., 120, https://doi.org/10.1002/2014JD022468, 2015b.

Plumb, R. A.: Stratospheric transport, J. Meteor. Soc. Japan, 80, 793–809, 2002.

Plumb, R. A. and Bell, R. C.: A model of the quasi-biennial oscillation on an equatorial beta-plane, Q. J. R. Meteorol. Soc., 108, 335–352, https://doi.org/10.1002/qj.49710845604, http://dx.doi.org/10.1002/qj.49710845604, 1982.

Pommrich, R., Müller, R., Grooß, J.-U., Konopka, P., Ploeger, F., B. Vogel, M. T., Hoppe, C. M., Günther, G., Spelten, N., Hoffmann, L., Pumphrey, H.-C., S. Viciani, F. D., Volk, C. M., Hoor, P., Schlager, H., and Riese, M.: Tropical troposphere to stratosphere transport of carbon monoxide and long-lived trace species in the Chemical Lagrangian Model of the Stratosphere (CLaMS), Geosci. Model Dev., 7, 2895–2916, https://doi.org/10.5194/gmd-7-2895-2014, 2014.

Punge, H. J., Konopka, P., Giorgetta, M. A., and Müller, R.: Effect of the quasi-biennial oscillation on low-latitude transport in the stratosphere derived from trajectory calculations, J. Geophys. Res., 114, D03 102, https://doi.org/10.1029/2008JD010518, 2009.

Randel, W. J., Garcia, R. R., Calvo, N., and Marsh, D.: ENSO influence on zonal mean temperature and ozone in the tropical lower stratosphere, Geophys. Res. Lett., 39, https://doi.org/10.1029/2009GL039343, 2009.

Reithmeier, C., Sausen, R., and Grewe, V.: Investigating lower stratospheric model transport: Lagrangian calculations of mean age and age spectra in the GCM ECHAM4, Clim. Dynam, 30, 225–238, https://doi.org/10.1007/s00382-007-0294-1, 2008.

Riese, M., Ploeger, F., Rap, A., Vogel, B., Konopka, P., Dameris, M., and Forster, P.: Impact of uncertainties in atmospheric mixing on simulated UTLS composition and related radiative effects, J. Geophys. Res., 117, D16305, https://doi.org/10.1029/2012JD017751, 2012.

Rosenlof, K. and Holton, J.: Estimates of the stratospheric residual circulation using the downward control principle, J. Geophys. Res., 98, 10,465–10,479, 1993.

Santee, M. L., Manney, G. L., Livesey, N. J., Schwartz, M. J., Neu, J. L., and Read, W. G.: A comprehensive overview of the climatological composition of the Asian summer monsoon anticyclone based on 10 years of Aura Microwave Limb Sounder measurements, J. Geophys. Res.: Atmos., 122, 5491–5514, https://doi.org/10.1002/2016JD026408, http://dx.doi.org/10.1002/2016JD026408, 2017.

Sassi, F., D., K., Boville, B. A., Garcia, R. R., and Roble, R.: Effect of El Niño Southern Oscillation on the dynamical, thermal, and chemical structure of the middle atmosphere, J. Geophys. Res.: Atmos., 109, https://doi.org/10.1029/2003JD004434, https://agupubs.onlinelibrary.wiley.com/doi/abs/10.1029/2003JD004434, 2004.

Scaife, A. A., Comer, R., Dunstone, N., Fereday, D., Folland, C., Good, E., Gordon, M., Hermanson, L., Ineson, S., Karpechko, A., Knight, J., MacLachlan, C., Maidens, A., Peterson, K. A., Smith, D., Slingo, J., and Walker, B.: Predictability of European winter 2015/2016, Atmos. Sci. Lett., 18, 38–44, https://doi.org/10.1002/asl.721, http://dx.doi.org/10.1002/asl.721, 2017.

Simpson, I. R., Shepherd, T. G., and Sigmond, M.: Dynamics of the Lower Stratospheric Circulation Response to ENSO, J. Atmos. Sci., 68, 2537–2556, https://doi.org/10.1175/JAS-D-11-05.1, https://doi.org/10.1175/JAS-D-11-05.1, 2011.

Solomon, S.: Stratospheric ozone depletion: A review of concepts and history, Rev. Geophys., 37, 275–316, https://doi.org/10.1029/1999RG900008, http://dx.doi.org/10.1029/1999RG900008, 1999.

Solomon, S., Rosenlof, K. H., Portmann, R. W., Daniel, J. S. Davis, S. M., Sanford, T., and Plattner, G.-K.: Contributions of Stratospheric Water Vapor to Decadal Changes in the Rate of Global Warming, Science, 327, 1219–1223, https://doi.org/10.1126/science.1182488, http://science.sciencemag.org/content/327/5970/1219, 2010.

Taguchi, M.: Observed connection of the stratospheric quasi-biennial oscillation with El Niño–Southern Oscillation in radiosonde data, J. Geophys. Res.: Atmos., 115, https://doi.org/10.1029/2010JD014325, http://dx.doi.org/10.1029/2010JD014325, 2010.

Taguchi, M. and Hartmann, D. L.: Increased Occurrence of Stratospheric Sudden Warmings during El Niño as Simulated by WACCM, J. Clim., 19, 324–332, https://doi.org/10.1175/JCLI3655.1, https://doi.org/10.1175/JCLI3655.1, 2006.

Thomason, L. W., Ernest, N., Millán, L., Rieger, L., Bourassa, A., Vernier, J.-P., Manney, G., Luo, B., Arfeuille, F., and Peter, T.: A global space-based stratospheric aerosol climatology: 1979–2016, Earth Sys. Sci. Data, 10, 469–492, https://doi.org/10.5194/essd-10-469-2018, https://www.earth-syst-sci-data.net/10/469/2018/, 2018.

Thompson, A. M., Witte, J. C., Hudson, R. D., Guo, H., Herman, J. R., and Fujiwara, M.: Tropical Tropospheric Ozone and Biomass Burning, Science, 291, 2128–2132, https://doi.org/10.1126/science.291.5511.2128, http://science.sciencemag.org/content/291/5511/2128, 2001.

Timmermann, A., Oberhuber, J., Bacher, A., Esch, M., Latif, M., and Roeckner, E.: El Niño, La Nina, and the Southern Oscillation, Nature, 398, 904–905, https://doi.org/10.1038/19505, http://dx.doi.org/10.1038/19505, 1999.

Trentmann, J., Luderer, G., Winterrath, T., Fromm, M. D., Servranckx, R., Textor, C., Herzog, M., Graf, H.-F., and Andreae, M. O.: Modeling of biomass smoke injection into the lower stratosphere by a large forest fire (Part I): reference simulation, Atmos. Chem. Phys., 6, 5247–5260, https://doi.org/10.5194/acp-6-5247-2006, https://www.atmos-chem-phys.net/6/5247/2006/, 2006.

Trepte, C. R. and Hitchman, M. H.: Tropical stratospheric circulation deduced from satellite aerosol data, Nat. Geosci., 355, 626–628, https://doi.org/10.1038/355626a0, http://dx.doi.org/10.1038/ngeo2138, 1992.

van Oldenborgh, G. J., Philip, S. Y., and Collins, M.: El Niño in a changing climate: a multi-model study, Ocean Science, 1, 81–95, https://doi.org/10.5194/os-1-81-2005, https://www.ocean-sci.net/1/81/2005/, 2005.

Vernier, J. P., Thomason, L. W., Pommereau, J. P., Bourassa, A., Pelon, J., Garnier, A., Hauchecorne, A., Trepte, C., Degenstein, D., and Vargas, F.: Major influence of tropical volcanic eruptions on the stratospheric aerosol layer during the last decade, Geophys. Res. Lett., 38, L12 807, https://doi.org/10.1029/2011GL047563, 2011.

von Storch, H. and Zwiers, F. W.: Statistical analysis in climate research, Cambridge Unv. Press, 1999.

Wang, C., Deser, Y. J.-Y., DiNezio, P., and Clement, A.: El Niño–Southern Oscillation (ENSO): A review. In Reefs of the Eastern Pacific, Springer Sci. Publish., pp. 85–106, 2016.

Waters, J. W., Froidevaux, L., Harwood, R. S., Jarnot, R. F., Pickett, H. M., Read, W. G., Siegel, P. H., Cofield, R. E., Filipiak, M. J., Flower, D. A., Holden, J. R., Lau, G. K., Livesey, N. J., Manney, G. L., Pumphrey, H. C., Santee, M. L., Wu, D. L., Cuddy, D. T., Lay, R. R., Loo, M. S., Perun, V. S., Schwartz, M. J., Stek, P. C., Thurstans, R. P., Boyles, M. A., Chandra, K. M., Chavez, M. C., Chen, G.-S., Chudasama, B. V., Dodge, R., Fuller, R. A., Girard, M. A., Jiang, J. H., Jiang, Y., Knosp, B. W., LaBelle, R. C., Lam, J. C., Lee, K. A., Miller, D., Oswald, J. E., Patel, N. C., Pukala, D. M., Quintero, O., Scaff, D. M., Van Snyder, W., Tope, M. C., Wagner, P. A., and Walch, M. J.: The Earth Observing System Microwave Limb Sounder (EOS MLS) on the Aura satellite, IEEE Trans. on Geosci. and Remote Sens., 122, 1075–1092, https://doi.org/10.1109/TGRS.2006.873771, 2006.

Waugh, D. and Hall, T.: Age of stratospheric air: Theory, observations, and models, Rev. Geophys., 40, 1010, https://doi.org/10.1029/2000RG000101, 2002.

WMO: Scientific Assessment of Ozone Depletion: 2014, Global ozone research and monitoring project - report no. 55, WMO (World Meteorological Organization), Geneva, http://www.wmo.int/pages/prog/arep/gaw/ozone_2014/full_report_TOC.html, 2014.

Wolter, K. and Timlin, M. S.: El Nino/Southern Oscillation behaviour since 1871 as diagnosed in an extended multivariate ENSO index (MEI.ext), Int. J. Climatol., 31, 1074–1087, https://doi.org/10.1002/joc.2336, 2011.

Wright, J. S. and Fueglistaler, S.: Large differences in reanalyses of diabatic heating in the tropical upper troposphere and lower stratosphere, Atmos. Chem. Phys., 13, 9565–9576, https://doi.org/10.5194/acp-13-9565-2013, https://www.atmos-chem-phys.net/13/9565/2013/, 2013.

Yang, H., Chen, G., and Domeisen, D. I. V.: Sensitivities of the Lower Stratospheric Transport and Mixing to Tropical SST Heating, J. Atmos. Sci., 71, 2674–2694, https://doi.org/10.1175/JAS-D-13-0276.1, 2014.

Yang, H., Chen, G., Tang, Q., and Hess, P.: Quantifying isentropic stratosphere-troposphere exchange of ozone, J. Geophys. Res.: Atmos., 121, 3372–3387, https://doi.org/10.1002/2015JD024180, https://agupubs.onlinelibrary.wiley.com/doi/abs/10.1002/2015JD024180, 2016.

Yulaeva, E. and Wallace, J. M.: The Signature of ENSO in Global Temperature and Precipitation Fields Derived from the Microwave Sounding Unit, J. of Clim., 7, 1719–1736, https://doi.org/10.1175/1520-0442(1994)007<1719:TSOEIG>2.0.CO;2, 1994.

Zhou, X., Li, J., Xie, F., Chen, Q., Ding, R., Zhang, W., and Li, Y.: Does Extreme El Niño Have a Different Effect on the Stratosphere in Boreal Winter Than Its Moderate Counterpart?, J. Geophys. Res.: Atmos., 123, 3071–3086, https://doi.org/10.1002/2017JD028064, https://agupubs.onlinelibrary.wiley.com/doi/abs/10.1002/2017JD028064, 2018.

Zwiers, F. W. and von Storch, H.: Taking Serial Correlation into Account in Tests of the Mean, J. of Clim., 8, 336–351, https://doi.org/10.1175/1520-0442(1995)008<0336:TSCIAI>2.0.CO;2, 1995.

Atmos. Chem. Phys. Discuss., https://doi.org/10.5194/acp-2018-688
Manuscript under review for journal Atmos. Chem. Phys.
Discussion started: 6 August 2018

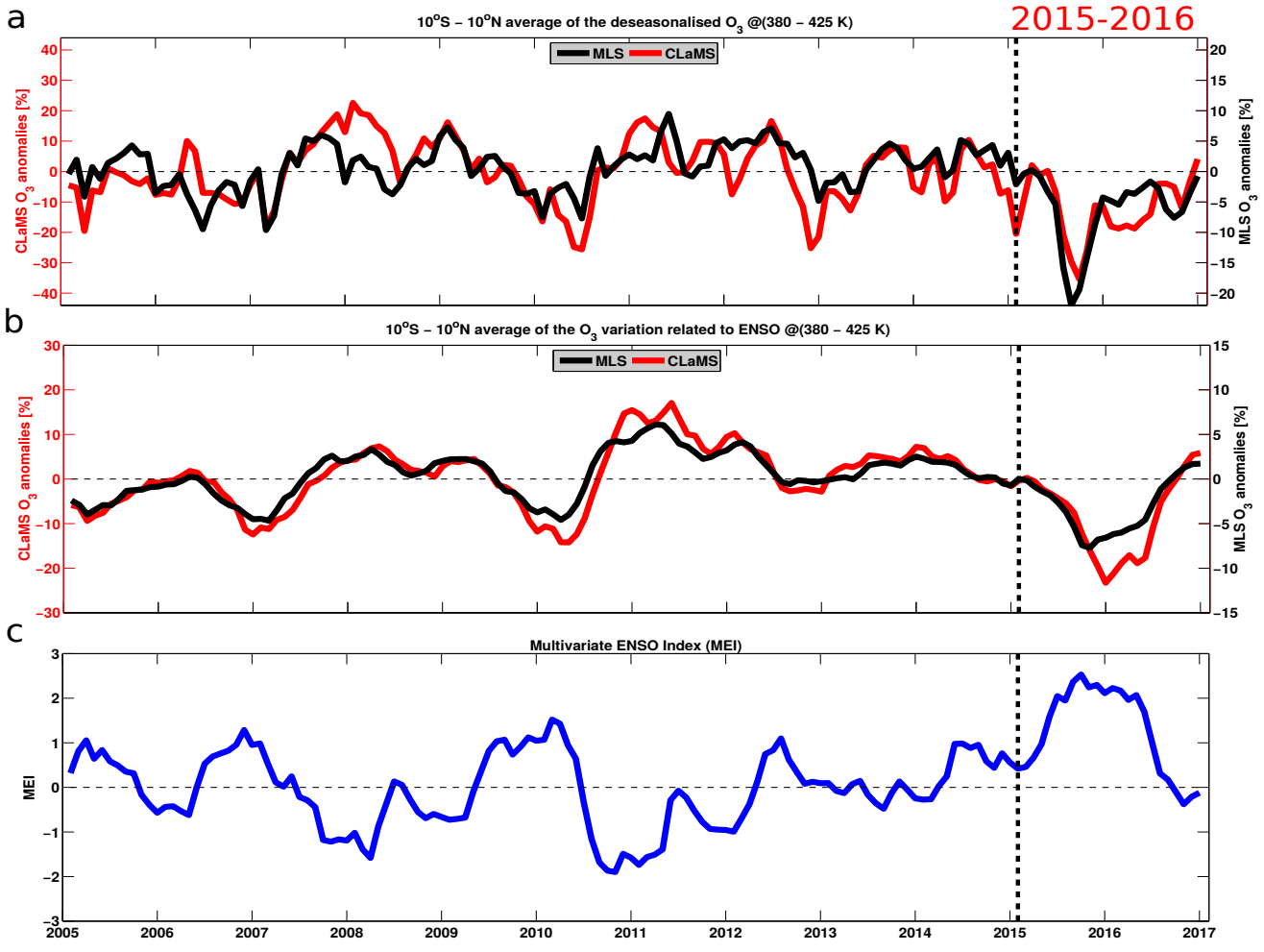

Figure 1. Time evolution of the tropical O_3 anomalies from CLaMS simulations and MLS satellite observations in percent change from the monthly zonal mean climatology and averaged between 380–425 K for the 2005–2016 period. Panel (a) shows the 10° S–10° N deseasonalised O_3 for CLaMS (black) and MLS (red). Panel (b) shows the ENSO-induced O_3 anomalies in the tropics for CLaMS (black) and MLS (red) derived from the multiple regression fit together with the MEI. Panel (c) shows the Multivariate ENSO Index (MEI: blue). Note that there is a factor of 2 difference in the color scales in Figs. 1a and 1b, reflecting the difference in the magnitude of the deseasonalised O_3 mixing ratio between CLaMS and MLS. Vertical black dashed line indicates February 2015 for the warm ENSO onset.

Atmos. Chem. Phys. Discuss., https://doi.org/10.5194/acp-2018-688
Manuscript under review for journal Atmos. Chem. Phys.
Discussion started: 6 August 2018

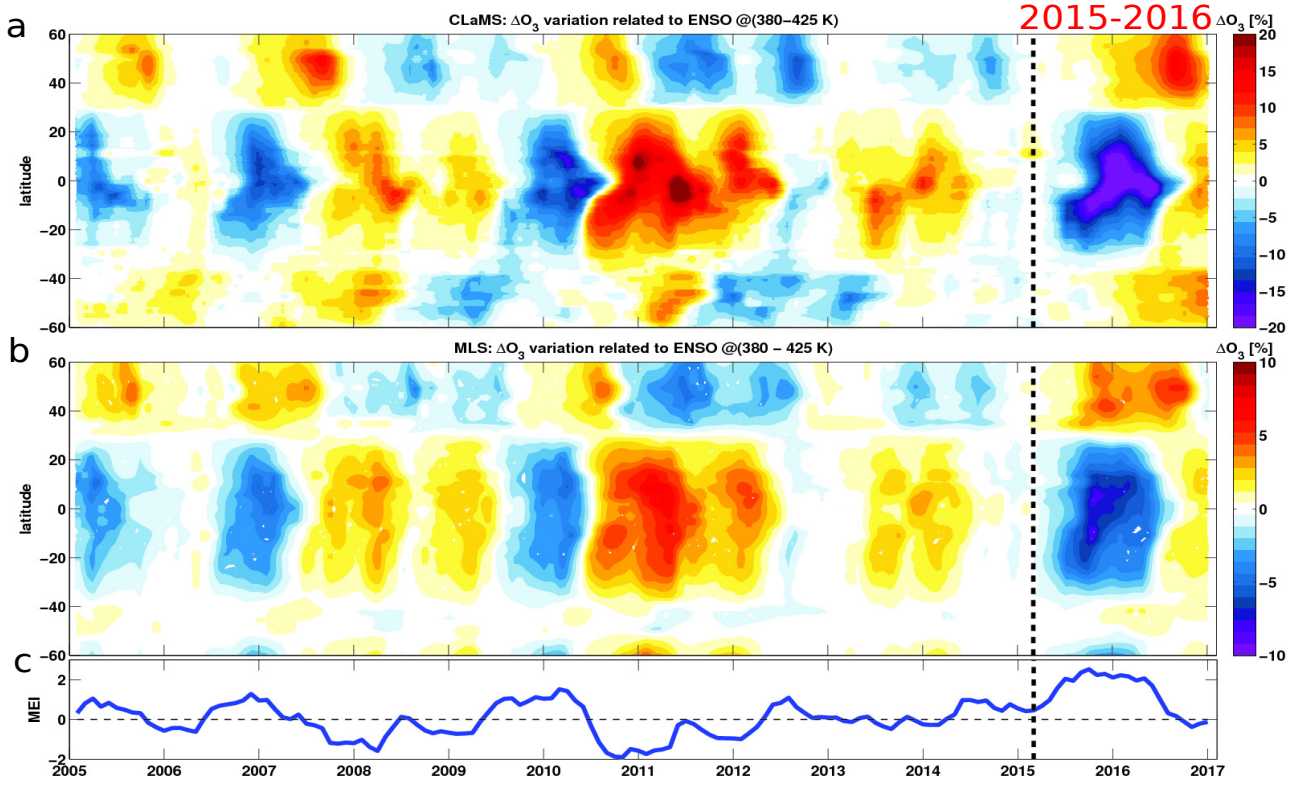

Figure 2. Latitude-time evolution of the ENSO impact on lower stratospheric O_3 from (a) CLaMS simulations and (b) MLS satellite observations in percent change from the monthly zonal mean climatology derived from the multiple regression fit and averaged between 380–425 K for the 2005–2016 period. Note that there is a factor of 2 difference in the color scales in Figs. 2a and 2b, reflecting the difference in the magnitude of the deseasonalised O_3 mixing ratio between CLaMS and MLS. The panel (c) shows the MEI in blue. Vertical black dashed line indicates February 2015 for the warm ENSO onset.

Atmos. Chem. Phys. Discuss., https://doi.org/10.5194/acp-2018-688
Manuscript under review for journal Atmos. Chem. Phys.
Discussion started: 6 August 2018

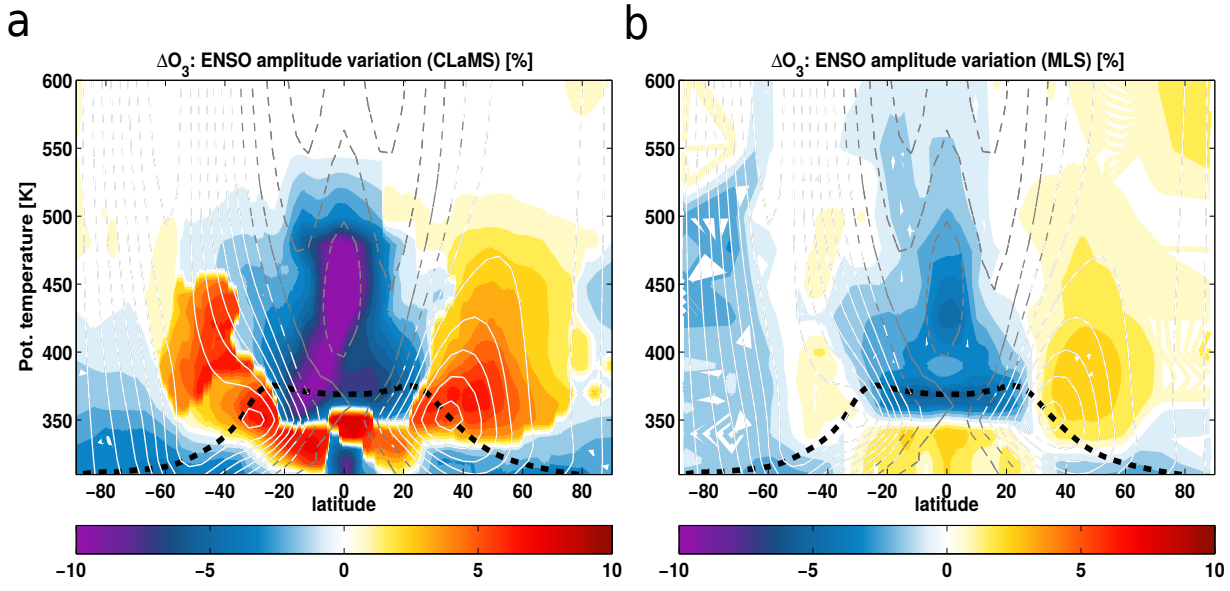

Figure 3. Zonal mean distribution of the ENSO impact on stratospheric O_3 variability from (a) CLaMS simulations and (b) MLS satellite observations in percent change relative to the climatological monthly mean mixing ratios. The amplitude of the O_3 variations (term $b_2 \times STD(MEI)$) attributed to ENSO is calculated by projecting the regression fits onto the ENSO basis functions for the 2005–2016 period. Black dashed horizontal line indicates the climatological tropopause from ERA-I. Zonal mean wind component, u ($m \cdot s^{-1}$), averaged over the 2015–2016 period, from ERA-I is overplotted as solid white (westerly) and dashed grey (easterly) lines.

Atmos. Chem. Phys. Discuss., https://doi.org/10.5194/acp-2018-688
Manuscript under review for journal Atmos. Chem. Phys.
Discussion started: 6 August 2018

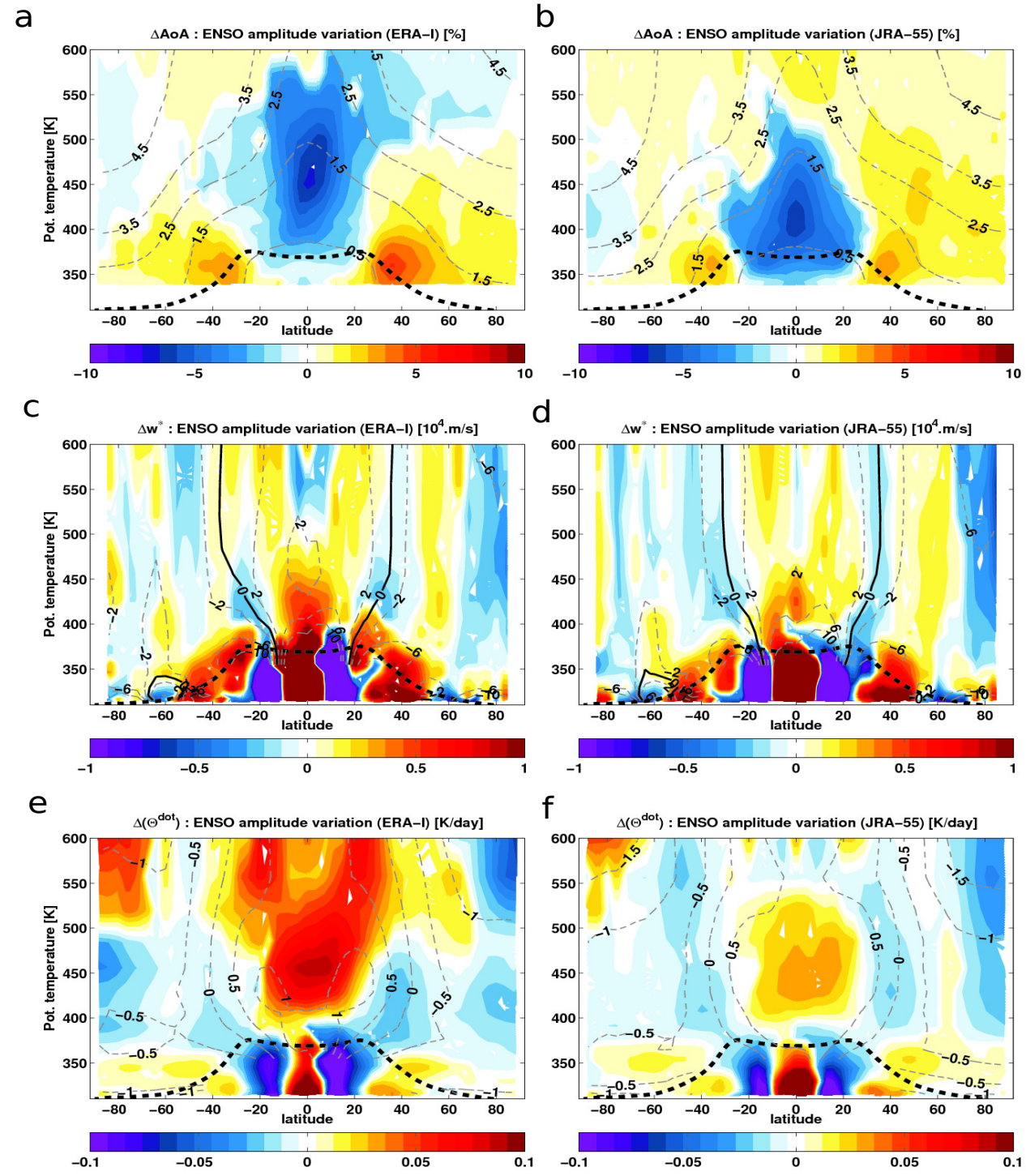

Figure 4. Zonal mean distribution of the ENSO impact on mean age (a, b), residual vertical velocity ($\overline{w^*}$) (c, d) and diabatic heating rate ($\dot{\Theta}$) (e, f) from CLaMS simulations driven by ERA-I and JRA-55 in percent change relative to the zonal monthly mean climatology. The amplitude of the O_3 variations (term $b_2 \times STD(MEI)$) attributed to ENSO is calculated by projecting the regression fits onto the ENSO basis functions for the 1979–2013 period. Black dashed horizontal line indicates the tropopause from ERA-I and JRA-55 reanalyses. Zonal mean climatologies of the mean age, $\overline{w^*}$ and $\dot{\Theta}$ are overplotted as dashed grey lines.

Atmos. Chem. Phys. Discuss., https://doi.org/10.5194/acp-2018-688
Manuscript under review for journal Atmos. Chem. Phys.
Discussion started: 6 August 2018

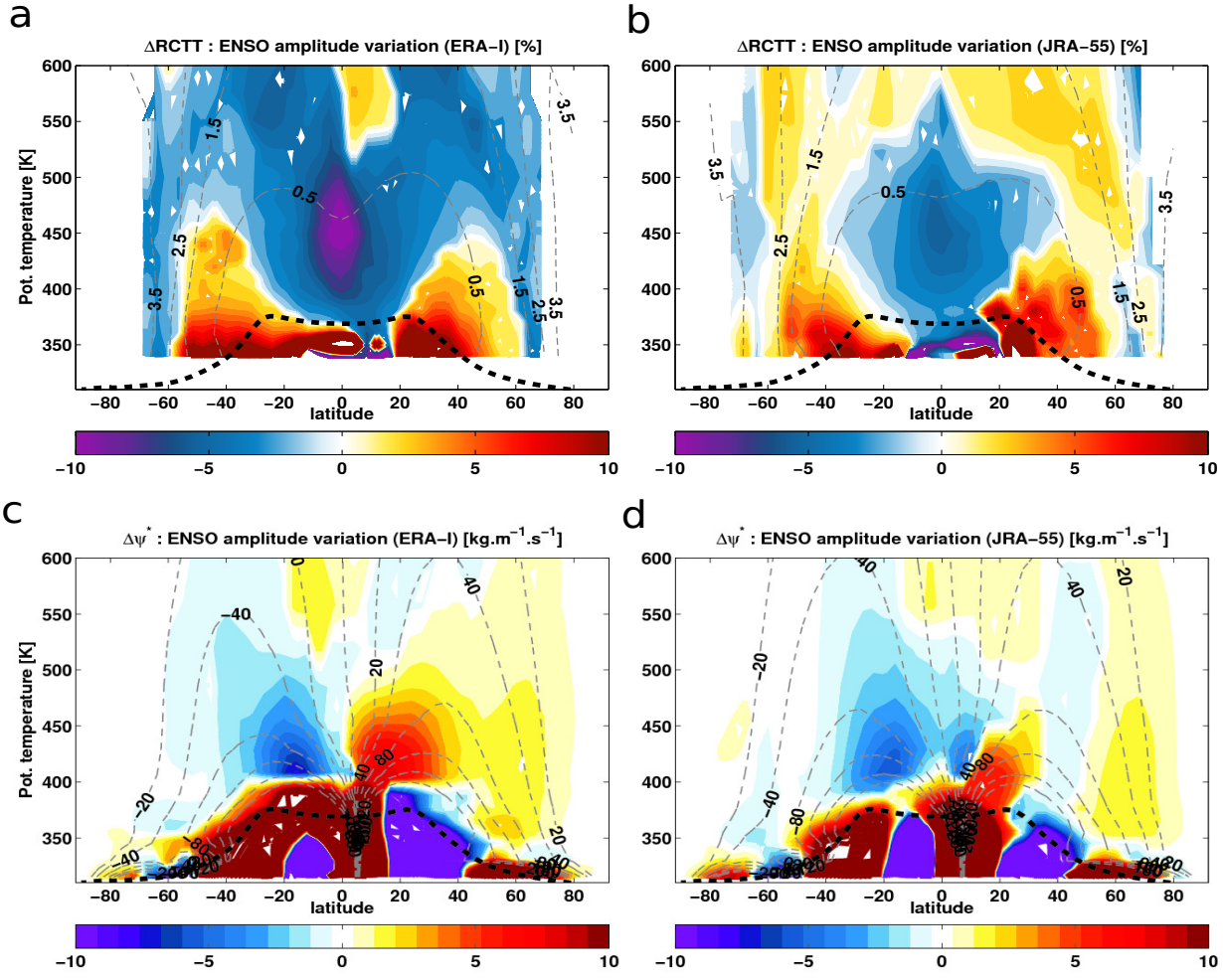

Figure 5. Zonal mean distribution of the ENSO impact on residual circulation transit time (RCTT) (a, b) and the residual circulation mass stream function (ψ^*) (c, d) from CLaMS simulations driven by ERA-I (a, c) and JRA-55 (b, d). RCTT is shown in percent change relative to the monthly zonal mean climatology. The amplitude of the RCTT and ψ^* variations (term $b_2 \times STD(MEI)$) attributed to the ENSO events is calculated by projecting the regression fits onto the ENSO basis functions for the 1979–2013 period. Black dashed horizontal line indicates the tropopause from ERA-I and JRA-55 reanalyses. Zonal mean climatology of the RCTT and ψ^* are overplotted as dashed grey lines.

Atmos. Chem. Phys. Discuss., https://doi.org/10.5194/acp-2018-688
Manuscript under review for journal Atmos. Chem. Phys.
Discussion started: 6 August 2018

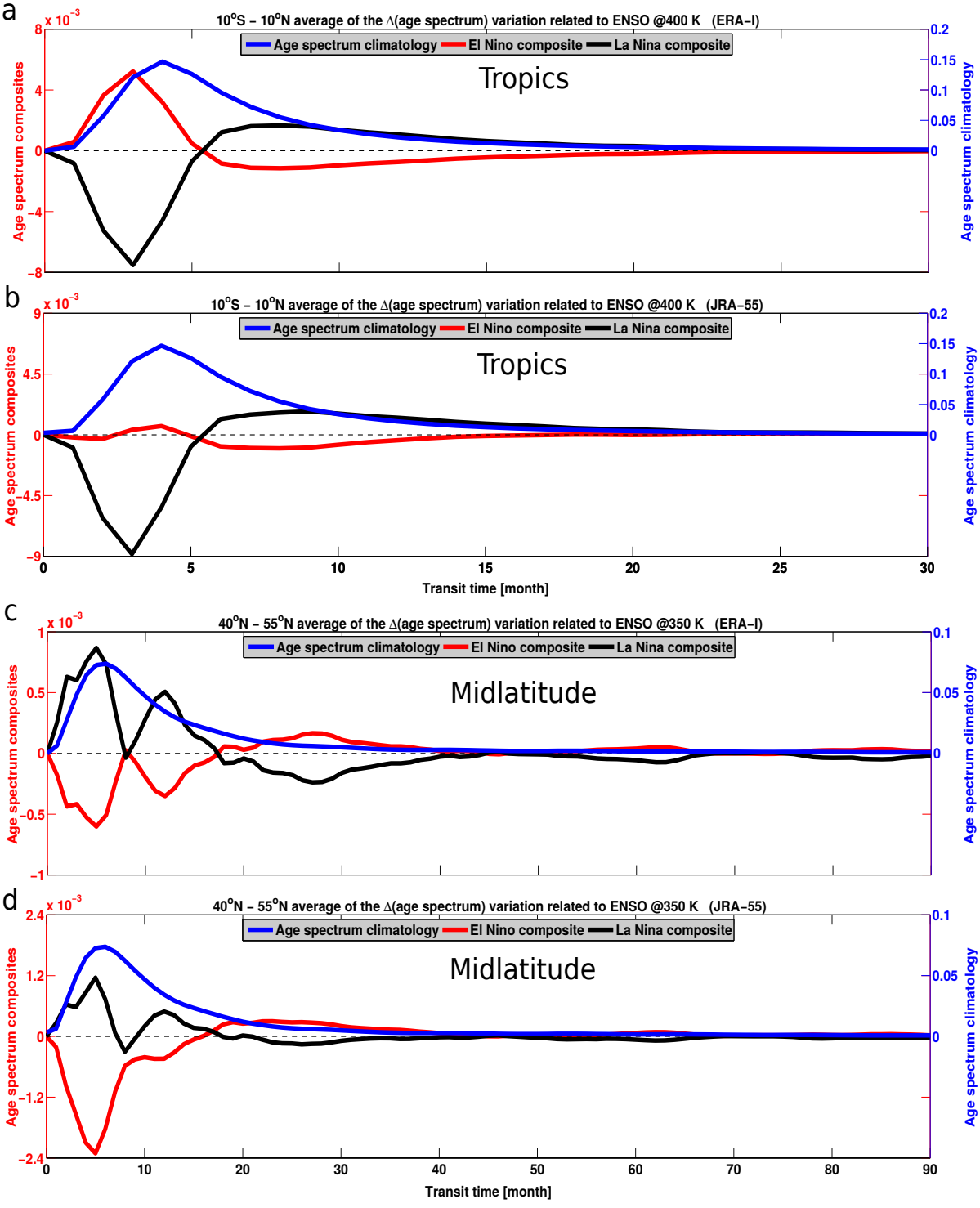

Figure 6. ENSO impact on monthly-mean age spectrum from CLaMS simulations driven by ERA-I and JRA-55 reanalyses for the 1979–2013 period: (a, b) tropics at 400 K and, (c, d) midlatitude at 350 K. Shown El Niño and La Niña composites are derived from the multiple regression fit as the difference between the residual (ε in (1)) without and with explicit inclusion of the ENSO signal. Note that the x-axis ranges for the two sets of panels are not the same. The x-axis ranges of the tropical panels stop at 30 months, while the x-axis ranges of the midlatitude panels stop at 90 months.

Atmos. Chem. Phys. Discuss., https://doi.org/10.5194/acp-2018-688
Manuscript under review for journal Atmos. Chem. Phys.
Discussion started: 6 August 2018

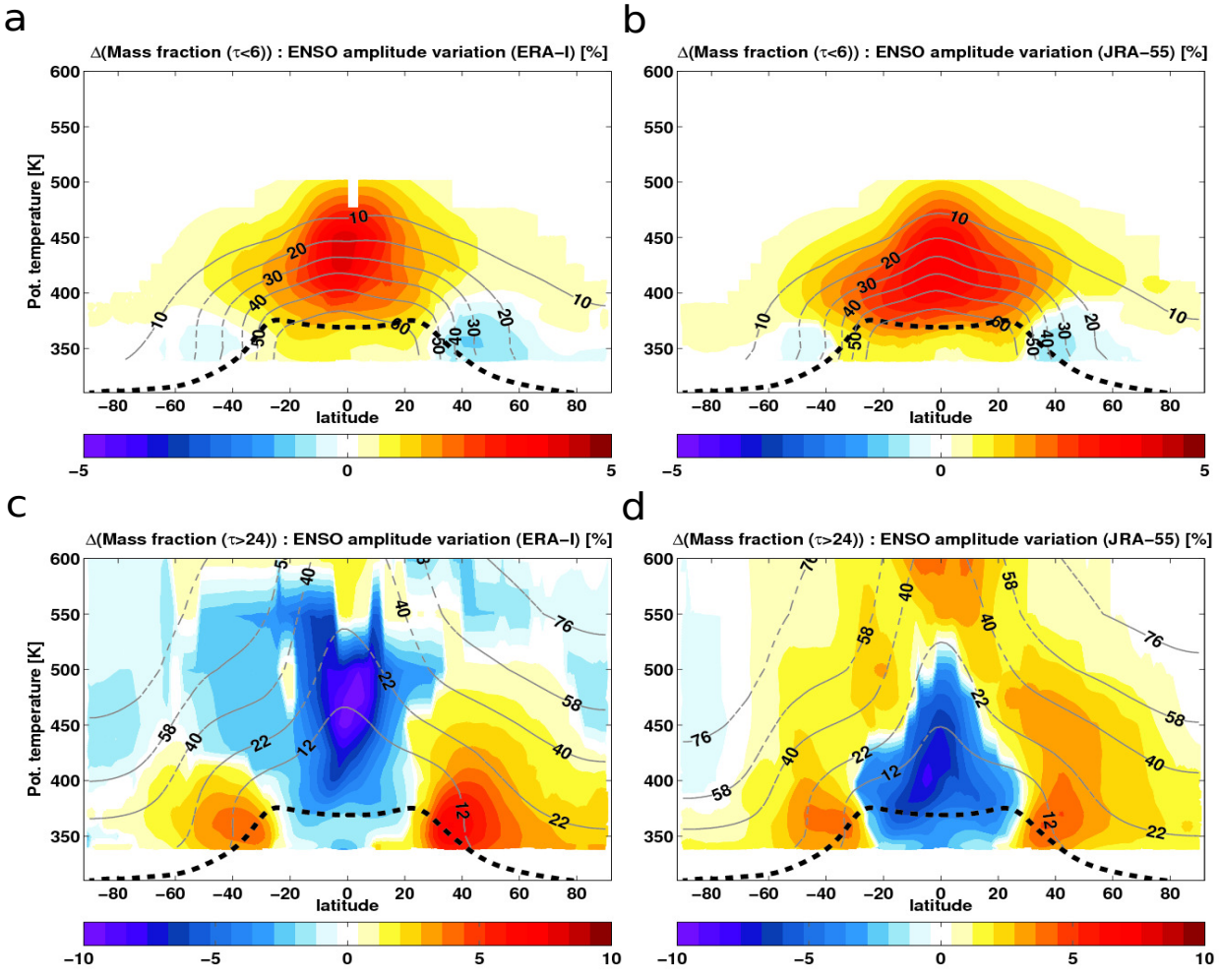

Figure 7. Zonal mean distribution of the ENSO impact on monthly-mean young and old air mass fraction from CLaMS simulations driven by (a, c) ERA-I and (b, d) JRA-55 reanalyses. The amplitude of the air mass fraction variations (term $b_2 \times STD(MEI)$) attributed to ENSO is calculated by projecting the regression fits onto the ENSO basis functions for the 1979–2013 period. ENSO amplitude variation of the young air mass fraction with transit time τ shorter than 6 months is shown in (a, b) panels. ENSO amplitude variation of the old air mass fraction with transit time τ longer than 24 months is shown in (c, d) panels. Grey contours are the climatology. Black dashed horizontal line indicates the tropopause from ERA-I and JRA-55 reanalyses.

Atmos. Chem. Phys. Discuss., https://doi.org/10.5194/acp-2018-688
Manuscript under review for journal Atmos. Chem. Phys.
Discussion started: 6 August 2018

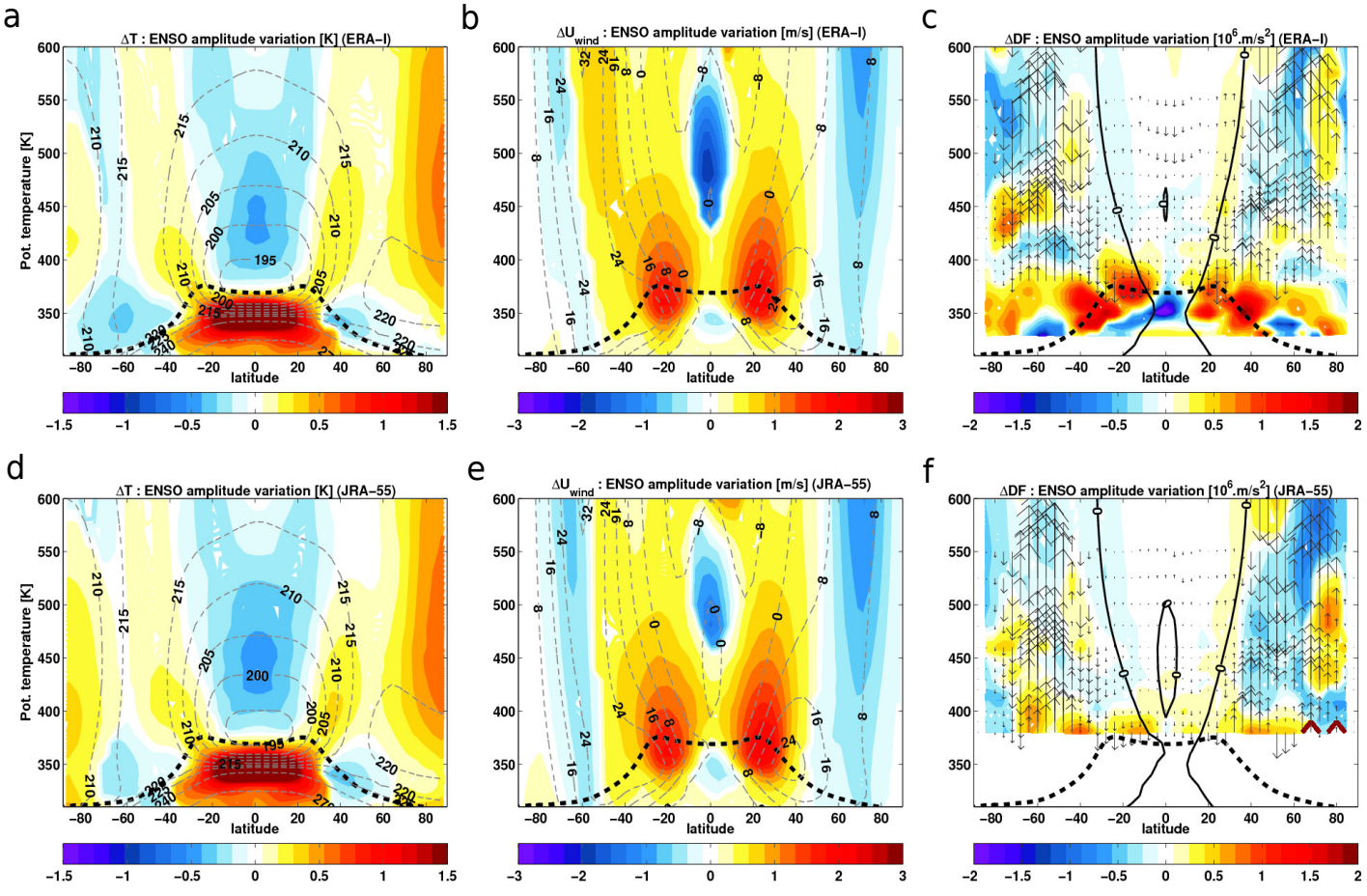

Figure 8. Zonal mean distribution of the ENSO impact on monthly-mean temperature [K], zonal wind [m/s] and EP-flux and its divergence [m.s^2] derived from (a–c) ERA-I and (d–f) JRA-55 reanalyses. The amplitude of the temperature, zonal wind and EP-flux variations (term $b_2 \times STD(MEI)$) attributed to the ENSO events is calculated by projecting the regression fits onto the ENSO basis functions for the 1979–2013 period. Black dashed horizontal line indicates the tropopause from ERA-I and JRA-55 reanalyses. Zonal mean climatologies are overplotted as dashed grey lines. The thick black line on Fig. 8(c, f) indicates the zero line wind. The arrows indicate the EP-Flux vectors.